

THE UTILITY OF IDEA-I AS A WILDFIRE SMOKE PLUME FORECAST TOOL: A MID-  
JULY 2014 CASE STUDY

by

Kyle M. Hosley

A thesis submitted in partial fulfillment of

The requirements for the degree of

Master of Science

(Department of Atmospheric and Oceanic Science)

At the

UNIVERSITY OF WISCONSIN-MADISON

2016

**APPROVED**

---

Signature

---

Date

Steven A. Ackerman  
Professor, Department of Atmospheric and Oceanic Sciences  
Director of the Cooperative Institute for Meteorological Satellite Studies  
University of Wisconsin-Madison  
Department of Atmospheric Science

## Abstract

New capabilities have been developed to forecast aerosol transport by aggregating trajectory output from the aerosol forecasting tool Infusing satellite Data into Environmental Applications - International (IDEA-I). These capabilities include estimates of aerosol optical depth (AOD) within the planetary boundary layer (PBL), cross-sections of extinction coefficient, and extinction coefficient profiles, all of which are obtained by aggregating multi-day IDEA-I trajectory forecasts. We compare results from these new capabilities with in situ surface measurements and satellite observations, including MODerate resolution Imaging Spectrometer (MODIS) AOD and true color imagery, AirNow fine particulate ( $PM_{2.5}$ ) observations, satellite-based lidar observations from the Cloud-Aerosol LIdar with Orthogonal Polarization (CALIOP) sensor, and surface-based lidar observations from the University of Wisconsin Space Science and Engineering Center (UW-SSEC) High Spectral Resolution Lidar (HSRL). We demonstrate these new capabilities by examining the period July 16 – July 20, 2014, which was when the most intense 3 day period of biomass burning in the continental United States (CONUS) during the spring and summer of 2014. The Deriving Information on Surface conditions from Column and Vertically Resolved Observations Relevant to Air Quality (DISCOVER-AQ) and Front Range Air Pollution and Photochemistry Experiment (FRAPPE) field missions along the Colorado Front Range coincided with this period, for which the UW-SSEC HSRL observed from the Boulder Atmospheric Observatory (BAO). Suggestions are presented for improving IDEA-I as an aerosol forecasting tool, with an emphasis on improving the forecasting of wildfire smoke plumes.

## Acknowledgements

The first person who I would like to thank is I would like to thank is my research advisor, Dr. R. Bradley Pierce, without whom this work would not be possible. I would also like to thank my academic advisor Dr. Steve Ackerman for his input during the writing and editing process. I also thank Dr. Tristan L'Ecuyer for reading my thesis and providing great feedback not only for my Master's thesis, but for future work as well. A special thanks goes out to Dr. Kathy Strabala and the rest of the IMAPP team for providing one year of funding for this research, for which I am grateful. I would also like to acknowledge Dr. Ed Eloranta and the UW Lidar Group for making the UW-SSEC HSRL data freely available. The HSRL data used in this study is a great resource. I would also like to thank colleague Marc Collins for his input during the editing process. I would also like to thank my parents for their support. Lastly, I would like to thank my fiancée for her support, as well as for her patience with me throughout this process.

## TABLE OF CONTENTS

|  |           |
|--|-----------|
| ABSTRACT.....  | i         |
| ACKNOWLEDGEMENTS.....  | ii        |
| TABLE OF CONTENTS.....   | iii       |
| <b>1. Introduction.....</b>  | <b>1</b>  |
| <b>2. Background.....</b>  | <b>3</b>  |
| 2.1 Satellites.....  | 3         |
| 2.2 The PM <sub>2.5</sub> /AOD Relationship.....                         | 5         |
| <b>3. Data.....</b>  | <b>10</b> |
| 3.1 Input Data Sets.....   | 10        |
| 3.2 Validation Data Sets.....  | 12        |
| <b>4. IDEA-I.....</b>  | <b>15</b> |
| 4.1 Requirements.....  | 15        |
| 4.2 Running IDEA-I.....  | 16        |
| 4.3 Assumptions in IDEA-I.....   | 17        |
| <b>5. Methods.....</b>   | <b>17</b> |
| 5.1 Optimization Test.....   | 18        |
| 5.2 Post-processing.....   | 19        |
| 5.2.1 Calculating PBL Top Pressure and Trajectory Point Height.....      | 20        |
| 5.2.2 Calculating Extinction Coefficient.....                            | 20        |
| 5.3 Trajectory Aggregation.....  | 21        |
| 5.4 Diagnostics.....   | 22        |
| 5.4.1 Forecast PBL AOD map.....  | 22        |
| 5.4.2 Scatter Plots and Time Series of PM <sub>2.5</sub> and AOD.....    | 23        |
| 5.4.3 Forecast Longitudinal Cross-Section of Extinction Coefficient..... | 23        |
| 5.4.4 Forecast Extinction Coefficient Point Profile.....                 | 24        |
| <b>6. Case Study.....</b>  | <b>24</b> |

|   |           |
|---|-----------|
| <b>7. Case Study Results.....</b>   | <b>26</b> |
| 7.1 Comparison of MODIS Imagery, AirNow PM <sub>2.5</sub> AQI, and Forecast PBL AOD Maps.....               | 27        |
| 7.1.1 July 16, 2014.....  | 27        |
| 7.1.2 July 17, 2014.....  | 29        |
| 7.1.3 July 18, 2014.....  | 31        |
| 7.1.4 July 19, 2014.....  | 32        |
| 7.1.5 July 20, 2014.....  | 34        |
| 7.2 Correlation Between Observed PM <sub>2.5</sub> and Forecast PBL AOD.....                                | 35        |
| 7.3 CALIOP Vertical Feature Mask Image vs. IDEA-I Longitudinal Cross-Section of Extinction Coefficient..... | 36        |
| 7.3.1 July 16, 2014.....  | 37        |
| 7.3.2 July 17, 2014.....  | 38        |
| 7.3.3 July 18, 2014.....  | 39        |
| 7.3.4 July 19, 2014.....  | 39        |
| 7.3.5 July 20, 2014.....  | 40        |
| 7.4 HSRL lidar observations vs. IDEA-I Forecast Extinction Coefficient Profile.....                         | 41        |
| <b>8. Discussion.....</b>   | <b>45</b> |
| 8.1 Spatial and Temporal Resolution of Input Data Sets.....   | 46        |
| 8.1.1 Meteorology.....  | 46        |
| 8.1.2 Aerosol Optical Depth.....  | 47        |
| 8.2 Inclusion of Fire Products.....   | 47        |
| 8.3 Inclusion of Physical Processes.....  | 48        |
| 8.4 Aerosol Homogeneity.....  | 49        |
| 8.5 Retrieval Restriction Due to Cloud Cover.....   | 49        |
| 8.6 The PM <sub>2.5</sub> /AOD Ratio.....   | 50        |
| <b>9. Conclusion.....</b>   | <b>51</b> |
| <b>10. Future Work.....</b>   | <b>51</b> |
| REFERENCES.....   | 53        |

## LIST OF TABLES

|                     |           |
|---------------------|-----------|
| <b>Table 1.....</b> | <b>57</b> |
|---------------------|-----------|

## LIST OF FIGURES

|                      |           |
|----------------------|-----------|
| <b>Figure 1.....</b> | <b>58</b> |
| <b>Figure 2.....</b> | <b>58</b> |

|                       |           |
|-----------------------|-----------|
| <b>Figure 3.....</b>  | <b>59</b> |
| <b>Figure 4.....</b>  | <b>60</b> |
| <b>Figure 5.....</b>  | <b>61</b> |
| <b>Figure 6.....</b>  | <b>62</b> |
| <b>Figure 7.....</b>  | <b>63</b> |
| <b>Figure 8.....</b>  | <b>64</b> |
| <b>Figure 9.....</b>  | <b>65</b> |
| <b>Figure 10.....</b> | <b>66</b> |
| <b>Figure 11.....</b> | <b>67</b> |
| <b>Figure 12.....</b> | <b>68</b> |
| <b>Figure 13.....</b> | <b>69</b> |
| <b>Figure 14.....</b> | <b>70</b> |
| <b>Figure 15.....</b> | <b>71</b> |
| <b>Figure 16.....</b> | <b>72</b> |
| <b>Figure 17.....</b> | <b>73</b> |
| <b>Figure 18.....</b> | <b>74</b> |
| <b>Figure 19.....</b> | <b>75</b> |
| <b>Figure 20.....</b> | <b>76</b> |
| <b>Figure 21.....</b> | <b>77</b> |
| <b>Figure 22.....</b> | <b>78</b> |
| <b>Figure 23.....</b> | <b>79</b> |
| <b>Figure 24.....</b> | <b>80</b> |
| <b>Figure 25.....</b> | <b>81</b> |

## 1. Introduction

Fine particulate matter (PM<sub>2.5</sub>), or aerosol that is less than 2.5 microns in diameter, is one of the six criteria air pollutants that the Environmental Protection Agency (EPA) regulates. As a pollutant regulated by the EPA, understanding the spatial distribution of surface PM<sub>2.5</sub> is vital for human health and regulatory policy. There currently exists a large network of air quality monitoring sites across the United States and Canada, most of which record PM<sub>2.5</sub> observations. Even though these networks have thousands of monitors, there are still regions which lack air quality monitoring sites. However, the use of satellite retrieved air quality measurements could remedy this issue. Information on aerosols retrieved from satellites has greatly aided the air quality community. The increase in spatial coverage from using surface-based observation networks to using satellite observations has allowed for easier tracking of pollution plumes, improvements in air quality forecasting, greater proof of exceptional events, and evaluation of air quality models (Duncan et al., 2014).

Infusing satellite Data into Environmental Applications - International (IDEA-I) is an open source satellite-based aerosol forecasting, visualization, and data synthesis tool intended for use by the international air quality forecasting community. IDEA-I is available for download from ([http://cimss.ssec.wisc.edu/imapp/ideai\\_v1.1.shtml](http://cimss.ssec.wisc.edu/imapp/ideai_v1.1.shtml)). IDEA-I uses MODerate resolution Imaging Spectroradiometer (MODIS; Justice et al., 1998; Esaias et al., 1998; Masuoka et al., 1998) satellite data to initialize a forward trajectory model, the Langley Research Center (LaRC) Trajectory Model (LaTM; Pierce and Fairlie, 1993; Pierce et al., 1994a; Pierce et al., 1994b; Pierce et al., 1997; Fairlie et al., 2009; Fairlie et al., 2014), the results of which can be used as a forecast (Al-Saadi, et al., 2005). In the field of air quality,

the two most problematic air pollutants are ozone and  $PM_{2.5}$ . Our study will only examine forecasting  $PM_{2.5}$ .

Our goal with this study is to improve the forecast of surface air quality using satellite observations of aerosols. The secondary goal is to also determine the validity of IDEA-I as a wildfire smoke plume forecast tool, as wildfire smoke plumes are associated with the emission of high  $PM_{2.5}$  concentrations. However, surface  $PM_{2.5}$  retrieval from satellite instruments is not possible. The only method by which one can obtain a value for surface  $PM_{2.5}$  from satellite observations is by estimating the value from retrievals of aerosol optical depth (AOD), a measure of how much aerosol exists between the satellite and Earth's surface. This estimate is a valid way to obtain surface  $PM_{2.5}$  because surface  $PM_{2.5}$  is a subset of aerosols and, where higher  $PM_{2.5}$  is observed, one can expect to observe higher aerosol in that column. However, the uncertainty of making such an estimate is approximately 30% (Hoff and Christopher, 2009). We wish to improve the uncertainty in the estimation of this value.

Since IDEA-I utilizes satellite data, no surface  $PM_{2.5}$  measurements are used and, thus, no forecasts of surface  $PM_{2.5}$  are made. Instead of forecasting surface  $PM_{2.5}$ , we decide to forecast which portion of the total column AOD lies within the PBL. Knowing what portion of the total aerosol column resides within the PBL is imperative to this study because PBL AOD can be used as a proxy for surface  $PM_{2.5}$ . There exists a positive relationship between PBL AOD and surface  $PM_{2.5}$ , but no relationship between lofted aerosol and surface  $PM_{2.5}$ . Since the PBL is usually well mixed, the PBL is in contact with the surface, and surface  $PM_{2.5}$  is a subset of aerosols, we can forecast PBL AOD in IDEA-I as a way to understand where we may expect to see the highest surface  $PM_{2.5}$  concentrations. In the next

section, we present a brief history of satellite remote sensing and a literature review of the  $PM_{2.5}$ /AOD relationship.

## **2. Background**

### ***2.1 Satellites***

The advent of satellite remote sensing of Earth's atmosphere changed atmospheric science forever. Before the advent satellites, only surface-based instruments, weather balloons, and aircraft observed Earth's atmosphere. These measurements provided valuable information to models, but they lacked broad spatial coverage, especially for upper-air observations. Satellites greatly increased the spatial coverage of observations by retrieving data over expansive regions of the globe at any one time. Satellites also allow us to see more atmospheric structures by using infrared, microwave, and a combination of wavelength channels to observe water vapor, temperature, and trace gas concentrations. Another important result of satellite remote sensing is the ability to observe nearly all locations on Earth's surface, including the oceans, the polar regions, and the most remote locations on land. As data from satellites are of great importance in this study, we present a brief history of the remote sensing of aerosols.

The operational aerosol-observing satellite era began in October of 1978, when both the TIROS-N and Nimbus-7 satellites were launched. Launched on October 19, 1978, the TIROS-N satellite was home to the Advanced Very High Resolution Radiometer (AVHRR) instrument, with the intent to provide solely meteorological data (Lee et al., 2009). Six days after the TIROS-N satellite was launched, the Total Ozone Mapping Spectrometer (TOMS;

Herman et al., 1997) was launched into space aboard the Nimbus-7 satellite. Like the AVHRR, TOMS initial capabilities did not include aerosol monitoring (Lee et al., 2009). However, TOMS would eventually become the instrument with the longest record of continuous global aerosol observation (Herman et al., 1997; Torres et al., 2002; Lee et al., 2009). Two other important launches early in the aerosol-monitoring satellite era are the Geostationary Operational Environmental Satellite (GOES), which housed the Visible Infrared Spin-Scan Radiometer (VISSR), and the NOAA-7, which had an updated AVHRR sensor (AVHRR/2) with an additional fifth spectral band. GOES/VISSR aerosol measurements were used in earlier regional studies (Fraser et al., 1984; King et al., 1999). The AVHRR Pathfinder Atmosphere (PATMOS) is a climate data set that is essentially calibrated AVHRR climate and aerosol data (Stowe et al., 2002). PATMOS has been used in numerous studies as a long-term record of atmospheric aerosols beginning in 1981 (Zhao et al., 2008; Streets et al., 2009). These early retrievals of aerosol laid the groundwork for the advancement of space-borne instruments currently observing the Earth.

In the nearly 40 years since AVHRR and TOMS were launched into an orbit around Earth onboard Landsat 1, remote sensing of aerosol in Earth's atmosphere has become much more sophisticated. Active sensors, such as the Cloud-Aerosol Lidar with Orthogonal Polarization (CALIOP) sensor aboard the Cloud-Aerosol Lidar and Infrared Pathfinder Satellite Observations (CALIPSO) satellite (Winker et al., 2004; Anderson et al., 2005; Holz et al., 2008; Winker et al., 2009), utilize sensing the returned power of an emitted pulse of energy to provide information on the vertical resolution of atmospheric aerosols. Passive sensors, such as MODIS, the Visible Infrared Imaging Radiometer Suite (VIIRS; Justice et al., 2013), and Multi-angle Imaging SpectroRadiometer (MISR; Diner et al., 1998),

utilize the reflectance of solar radiation to determine aerosol properties over a given location. A discussion of the MODIS and CALIOP sensors, as well as the platforms on which they reside (Terra/Aqua and CALIPSO, respectively) is given in later sections, as both MODIS and CALIOP data are employed in this study.

Passive satellite sensors are capable of observing the total amount of aerosol in a column (AOD), but lack the vertical resolution needed for the accurate monitoring of surface air quality. Active satellite sensors can provide vital information on the vertical distribution of aerosols, but the sensors only capture small portions of Earth's atmosphere at one time. This results in much of Earth unseen by any single active sensor. Another complicating issue in retrieving AOD is the inhomogeneity of aerosols. The microphysical properties of aerosols from different sources, including size distribution, shape, phase and water content, can be quite dissimilar and can drastically affect the optical properties of an aerosol column. Passive sensors must make certain assumptions about these microphysical quantities in order to determine the AOD value. In addition to the microphysical properties of aerosols, larger scale features such as planetary boundary layer (PBL) height, vertical distribution, and mixing can affect these properties as well (Hoff and Christopher, 2009; Li et al., 2011). Two other complicating factors in space borne passive retrieval of near-surface particulate matter are the constant natural and anthropogenic emission of fine particulates at the surface and stronger atmospheric scattering from the denser lower troposphere limiting sensitivity to radiation from the PBL (Martin, 2008).

## ***2.2 The PM<sub>2.5</sub>/AOD relationship***

AOD is the most readily available remotely sensed property of aerosols. AOD is a column measurement with no vertical information. As stated earlier, the only valid way to

determine the surface  $PM_{2.5}$  concentrations using satellites is to estimate surface  $PM_{2.5}$  values using a ratio between  $PM_{2.5}$  and AOD (Gupta and Christopher, 2009a). To investigate the  $PM_{2.5}$  to total column AOD (P/A) relationship, one needs to compare surface  $PM_{2.5}$  observations to co-located satellite retrievals of AOD. This task has been performed in numerous papers studying a wide variety of times and locations (Wang and Christopher, 2003; Engel-Cox et al., 2004; Hutchison et al., 2005; Engel-Cox et al., 2006; Hutchison et al., 2007; Gupta and Christopher, 2008; Gupta and Christopher, 2009a; Gupta and Christopher, 2009b; Hoff and Christopher, 2009; Zhang et al., 2009). The inherent characteristics of aerosols and the variability in the environment make the accurate prediction of the P/A relationship very difficult. Variance enters the calculation of the P/A ratio through many means: the properties of the observed aerosols, the environment of region of interest, and the surface cover of the region of interest. Since one of the objectives of this study is to improve the ability to forecast surface  $PM_{2.5}$ , we present a review of the study of the relationship between  $PM_{2.5}$  and total column AOD.

Wang and Christopher (2003) examined the P/A ratio at the locations of seven different surface  $PM_{2.5}$  monitors throughout Jefferson County, Alabama and found good correlation between the two quantities ( $r=0.7$ ). This correlation is even greater ( $r>0.9$ ) when examining monthly averaged  $PM_{2.5}$  and AOD, especially during summer months. Space and surface based lidar data was also used to enhance the satellite data used. Wang and Christopher also put forth a method binning the data by surface  $PM_{2.5}$  measurements, with highly correlated results ( $r=0.98$ ).

Engel-Cox et al. (2004) examined the P/A ratio for different locations across the United States for the period beginning April 1, 2002 and ending September 30, 2002. They

found that the greatest correlations between  $PM_{2.5}$  and AOD in the United States occur east of  $100^{\circ}W$  and that dense smoke events can be misconstrued as cloud cover in satellite AOD retrievals. A follow up paper (Engel-Cox et al., 2006) added the use of lidar in the determination of their correlations, as well as making the assertion that lower correlations between  $PM_{2.5}$  and AOD are an indication of lofted aerosols.

Hutchison et al. (2005) found low correlation between surface  $PM_{2.5}$  and MODIS AOD across the state of Texas for a three month period in 2003 and all of 2004. A follow up paper (Hutchison et al., 2007) demonstrated that their results had improved significantly. Hutchison et al., 2007 state that a minimum number of MODIS retrievals are necessary to reduce cloud contamination as well as stating that meteorology is related to the pollution type and source. Knowing the source of pollution would allow for a more accurate representation of the microphysical properties of the aerosols present and, thus, the surface concentrations of fine particulates.

Gupta and Christopher (2008) used Terra MODIS AOD and  $PM_{2.5}$  data from EPA for the North Birmingham air quality monitor between February 24, 2000 and June 30, 2006 to investigate remote sensing of  $PM_{2.5}$ . They investigated the differences between using hourly and daily  $PM_{2.5}$  data, the impact of removing  $PM_{2.5}$  data for times when AOT data is invalid or unavailable, and the trends in air pollution over north central Alabama. Their results showed that using hourly  $PM_{2.5}$  data increases the correlation with MODIS AOT as opposed to daily  $PM_{2.5}$  data, removing  $PM_{2.5}$  data for missing or invalid AOT retrievals only decreases average  $PM_{2.5}$  by approximately  $2.2\mu g/m^3$ , and decreasing levels of  $PM_{2.5}$  are observed over the North Birmingham air monitor. They do state that the use of satellite data is quite useful

in  $PM_{2.5}$  monitoring at this location, but the results are only valid for the Birmingham area and may not be applicable to other regions.

Gupta and Christopher in 2009 released a two-part paper describing two separate methods by which one could examine the  $PM_{2.5}$  – AOD relationship. The first paper utilizes a multiple regression approach, while the second utilizes a neural network approach to investigate the  $PM_{2.5}$  – AOD relationship. Surface  $PM_{2.5}$  measurements from AirNow sites, Terra MODIS AOD retrievals, and hourly meteorological data from rapid update cycle (RUC) reanalyses from 2004, 2005, and 2006 are used in both the multiple regression and neural network approach papers. The main result from the multiple regression paper is that significant improvement (20%-50%) in the root-mean-square-error (rms-error) in the  $PM_{2.5}$  - AOD relationship is observed when temperature and PBL height are included. The main result from the second paper is that the artificial neural network (ANN) method performs better ( $r=0.74$  for hourly  $PM_{2.5}$ ;  $r=0.84$  for daily  $PM_{2.5}$ ) than the simple correlation ( $r=0.60$ ) and multiple regression ( $r=0.68$ ) methods. They also found that, as in Wang and Christopher (2003), the best agreement occurs during the summer months.

Hoff and Christopher (2009) investigated remote sensing of tropospheric pollution. Focusing mostly on aerosol in the form of AOD, Hoff and Christopher find that AOD measurements are precise to within  $\pm 20\%$  and  $PM_{2.5}$  derived from AOD retrievals is precise to within  $\pm 30\%$ , both uncertainties too large to use in air quality regulatory applications. Hoff and Christopher also compiled a list of 15 studies examining the P/A ratio. These 15 studies covered a wide range of domains, ranging from cities (Baltimore, St. Louis, and Beijing) to regions (Texas, Italy, and France) to continents (Europe and the entire United States). The results of this review show that there is great variance in the  $PM_{2.5}$  – AOD relationship,

depending on the region, the number of surface monitors used, the period of study, and the measurement period. However, if studies only using hourly  $PM_{2.5}$  are used to calculate the P/A ratio, the variance relative to a mean of  $33.8\mu\text{g}/\text{m}^3$  is approximately  $14.2\mu\text{g}/\text{m}^3$ . However, in this calculation, we exclude the Schaap et al. (2009) study because the resulting  $PM_{2.5}$  relationship is an outlier and data from only one monitor (Cabauw, Netherlands) was used. If one calculates the mean and variance further omitting the P/A ratio from Al-Saadi et al. (2005), the mean decreases modestly to  $28.16\mu\text{g}/\text{m}^3$  while the variance decreases considerably to  $3.6\mu\text{g}/\text{m}^3$ . The five remaining P/A estimates after the omission of outliers include studies from Baltimore, Beijing, the southeastern United States, France, and the entire contiguous United States (CONUS). As the remaining studies cover a wide array of domain sizes and locations, this is evidence for the existence of a global P/A value between  $25\mu\text{g}/\text{m}^3$  and  $30\mu\text{g}/\text{m}^3$ .

Zhang et al. (2009) examined hourly  $PM_{2.5}$  measurements and Terra MODIS AOD across the United States for the years of 2005 and 2006. Their investigation into regional (EPA regions)  $PM_{2.5}$  – AOD relationships reveal that the southeastern United States (EPA Region 4) has the best correlation between  $PM_{2.5}$  and AOD ( $r=0.6$ ), while the southwestern United States (EPA region 9) exhibits the weakest correlation ( $r=0.2$ ). The  $PM_{2.5}$  - AOD correlations are also greater in the summer and fall months. Zhang et al. (2009) also compare two different versions of the Terra AOD product (v4.0.1 and v5.2.6) and find the v5.2.6 AOD product correlates better with observations than the v4.0.1 product, but the cloud-screening algorithm lessens the areal coverage of the product.

Li et al. (2011) analyzed MODIS AOD retrievals, NCEP reanalysis meteorological data, and  $PM_{10}$  data from surface monitors across China and Thailand between 2001 and

2009 using simple and multiple regression techniques. They find that for China, like a number of studies done in the United States (Wang and Christopher, 2003; Gupta and Christopher, 2009a; Zhang et al., 2009), the summer months exhibit greater correlation than in other months. However, for the stations located in northern Thailand, the drier months (winter and spring) exhibit the greater correlations due to a much lower probability of cloud contamination than in the wetter summer and autumn months. They also find that meteorology, in particular relative humidity, has a major impact on the AOT-PM<sub>10</sub> relationship. Studies done in the United States (Hutchison et al., 2007; Gupta and Christopher, 2009a) support the finding that meteorology affects the AOD-PM<sub>2.5</sub> (or AOT-PM<sub>10</sub>) relationship.

### **3. Data**

#### ***3.1 Input Data Sets***

In order to run IDEA-I, two sets of data are necessary as input: satellite retrievals of AOD and meteorological forecasts including wind speed, wind direction, and pressure. For our study, we use Terra and Aqua MODIS 550nm AOD and the Global Forecast System (GFS) model zero-hour forecast as our meteorological data set. The next three paragraphs describe each of these data sets in detail.

MODIS is a set of two spectroradiometers aboard the Terra and Aqua satellites. Terra, launched into space in December 18, 1999, passes over the equator from north to south at 10:30am local time while Aqua, launched on May 4, 2002, passes over the equator from south to north at 1:30pm local time. MODIS sensors scan in 36 different spectral bands,

ranging from 0.4  $\mu\text{m}$  to 14.5 $\mu\text{m}$ . One scan of the MODIS instrument results in a swath of data 2330 km cross-track and 10km along track (Barnes et al., 1998; Masuoka et al., 1998). With the 36 channels available, numerous land, ocean, and atmospheric products are available (Justice et al., 1998; Esaias et al., 1998; Masuoka et al., 1998). One of the more widely used products, which is the one used in this study, is the aerosol optical depth product, validated by Chu et al. (2002) for over land retrievals and Remer et al. (2002) for over ocean retrievals. Aerosol optical depths are retrieved using seven different wavelengths (nm): 470, 555, 659, 865, 1240, 1640, and 2130 (Tanré et al., 1997). Also used are the 3.8  $\mu\text{m}$  and 11  $\mu\text{m}$  wavelength bands (Kaufman et al., 1997). However, most aerosol optical depth plots, including ours, are made using the 555nm (0.55 $\mu\text{m}$ ) band (Tanré et al., 1997; Chu et al., 2002; Remer et al., 2002).

The AOD retrievals we utilize in IDEA-I are 10 km resolution MODIS Level 2 Aerosol products from both the Terra (MOD04\_L2) and Aqua satellites (MYD04\_L2). All MOD04\_L2 and MYD04\_L2 retrievals were obtained from the Level 1 & Atmosphere Archive and Distribution System (LAADS) Web (<https://ladsweb.nascom.nasa.gov/data/search.html>). Within each of these retrievals is the parameter Optical\_Depth\_Land\_and\_Ocean, the variable IDEA-I extracts as the AOD values. Optical\_Depth\_Land\_and\_Ocean contains the AOD at 0.55 $\mu\text{m}$  over both land surfaces and ocean surfaces. These retrievals are used to initialize the LaTM within IDEA-I. In addition to the LAADS AOD retrievals, Cloud Optical Thickness (COT) retrievals are also obtained. The cloud images are illustrated in the initial AOD image output by IDEA-I. Aqua MODIS AOD and Aqua MODIS True Color Red-Green-Blue (RGB) images used in this study are obtained from the operational IDEA page at the NOAA Center for Satellite

Applications and Research (STAR) National Environmental Satellite, Data, and Information Service (NESDIS; <http://www.star.nesdis.noaa.gov/smcd/spb/aq/>).

The meteorological data used in IDEA-I are 0.5° resolution GFS model analyses (hour 000) with 26 prescribed pressure levels from 1000mb to 10mb, with all data for a given run and forecast hour available in GRIB2 format (Kanamitsu, 1989; Kalnay et al., 1990, Kanamitsu et al., 1991). The GFS meteorological data is acquired by the IDEA-I script through a File Transfer Protocol (FTP) server at NOAA's National Operational Model Archive & Data Service (NOMADS) (<ftp://nomads.ncdc.noaa.gov/GFS/Grid4/201407/>). IDEA-I fetches the hour 000 GRIB2 file for each GFS run interval between 12Z July 16, 2014 and 00Z July 23, 2014. For each GRIB2 file, there is a similarly named inventory file which allows any user to explore what variables are stored in the GRIB2 file. In this study, the variables which will be used are the height of each prescribed pressure level, the pressure at those levels, the U and V wind components, vertical velocity (below 100mb only), and the height of the PBL. The horizontal and vertical wind components, as well as pressure, are necessary to run the LaTM within IDEA-I, whereas the pressure, height, and PBL height variables are all used in the post-processing of the IDEA-I output.

### ***3.2 Validation Data Sets***

In order to assess the viability of IDEA-I as a reliable smoke plume trajectory forecast tool, validation data sets are needed. For this study, we use AirNow surface observations of PM<sub>2.5</sub>, Cloud-Aerosol Lidar with Orthogonal Polarization (CALIOP) aerosol backscatter measurements, and HSRL aerosol backscatter measurements. We will describe these data sets in detail over the following paragraphs.

The hourly PM<sub>2.5</sub> surface observations are obtained from the United States EPA's AirNow network for the period beginning July 1, 2014 and ending August 31, 2014. For this period, 893 monitoring stations throughout the US and Canada have valid PM<sub>2.5</sub> surface observations. For each observation in the data file, the Site ID, the coordinates of the site, the name of the site, the date and time, and the PM<sub>2.5</sub> value are given. The AirNow data set is used to assess the relationship between the portion of the predicted AOD that resides within the PBL and hourly PM<sub>2.5</sub> surface observations. The AirNow PM<sub>2.5</sub> observations are recorded by either Federal Reference Method (FRM) or Federal Equivalence Method (FEM) monitors, such as Tapered Element Oscillating Microbalance (TEOM) and Beta Attenuation Monitor (BAM) instruments

(EPA - <http://www3.epa.gov/ttnamti1/files/ambient/pm25/r-98-012.pdf>). AirNow also creates and archives daily average PM<sub>2.5</sub> Air Quality Index (AQI) maps. There are six different levels of health concern for AQI ranges: Good (Green; 0 – 50; 0 – 12.0µg/m<sup>3</sup>), Moderate (Yellow; 51 – 100; 12.1 – 35.4µg/m<sup>3</sup>), Unhealthy for Sensitive Groups (USG; Orange; 101 – 150; 35.5 – 55.4µg/m<sup>3</sup>), Unhealthy (Red; 151 – 200; 55.5 – 150.4µg/m<sup>3</sup>), Very Unhealthy (Purple; 201 – 300; 150.5 – 250.4µg/m<sup>3</sup>), and Hazardous (Maroon; 301 – 500; 250.5 – 500.4µg/m<sup>3</sup>). Table 1 summarizes the PM<sub>2.5</sub> AQI. The AQI maps used in this study are obtained from the AirNow archive website

(<https://www.airnow.gov/index.cfm?action=airnow.mapsarchivecalendar>).

CALIOP is a dual wavelength lidar used to sample the atmosphere for clouds and aerosol. The dual wavelength lidar utilized by CALIOP is a neodymium-doped yttrium aluminum garnet (Nd:YAG) laser which simultaneously emits 1064nm and 532nm wavelength pulses approximately 20 times every second. CALIOP utilizes the information

obtained from the simultaneous pulses to create atmospheric profiles of attenuated backscatter, linear depolarization, and depolarization ratio along CALIPSO's track (Winker et. al. 2004; Anderson et. al., 2005; Holz et. al. 2008; Winker et. al. 2009). For this study, we obtain images of the vertical feature mask that coincide with CALIPSO overpass of the CONUS and southern Canada for the time period of interest (00Z July 16, 2014 – 00Z July 21, 2014; [http://www-calipso.larc.nasa.gov/products/lidar/browse\\_images/show\\_calendar.php](http://www-calipso.larc.nasa.gov/products/lidar/browse_images/show_calendar.php)). In the vertical feature mask images, we are most interested in any orange features (#3 – Aerosol), with mild interest in any brown features (#3L – Aerosol, Low Confidence). These images are compared to the longitudinal cross sections created using the trajectory aggregation method explained in the Methods section.

The final validation data set used in this experiment is the 41 day (July 9-August 18, 2014) record of the University of Wisconsin (UW) Space Science and Engineering Center's (SSEC) High Spectral Resolution Lidar (HSRL, Grund and Eloranta, 1991) measurements taken at the Boulder Atmospheric Observatory (BAO) in Erie, Colorado [(40N, 105W), <http://www.esrl.noaa.gov/psd/technology/bao/site/>]. The UW-SSEC HSRL is part of the set of instrumentation aboard the SSEC Portable Atmospheric Research Center (SPARC), SSEC's mobile laboratory deployed to the BAO in support of the FRAPPE field mission. The UW-SSEC HSRL measures backscatter, linear depolarization, 1064nm/532nm aerosol backscatter ratio, and 1064nm/532nm combined count ratio. The HSRL data recorded from the FRAPPE field mission are available for download in 81 separate, ready-to-download 12 hour time-height plots for each of the four variables listed above ([http://hsrl.ssec.wisc.edu/by\\_site/23/bscat/2014/07/](http://hsrl.ssec.wisc.edu/by_site/23/bscat/2014/07/) and

[http://hsrl.ssec.wisc.edu/by\\_site/23/bscat/2014/08/](http://hsrl.ssec.wisc.edu/by_site/23/bscat/2014/08/)). Customizable images can also be obtained from the HSRL website ([http://hsrl.ssec.wisc.edu/by\\_site/23/custom\\_rti/](http://hsrl.ssec.wisc.edu/by_site/23/custom_rti/)) dedicated to providing data from the HSRL lidar recorded during FRAPPE field mission. We utilized this service to obtain an image for the period of interest up to a height of ten kilometers. This data set is used in a qualitative comparison with similar images generated using output from IDEA-I.

## **4. IDEA-I**

### ***4.1 Requirements***

As stated in the introduction, IDEA-I is a satellite-based aerosol visualization and forecast tool. IDEA-I is available for download from the International MODIS/AIRS Processing Package (IMAPP) website ([http://cimss.ssec.wisc.edu/imapp/ideai\\_v1.1.shtml](http://cimss.ssec.wisc.edu/imapp/ideai_v1.1.shtml)). In order to run IDEA-I, one must first download the IDEA-I software package from the link provided. Additional requirements for running the IDEA-I software package are a CentOS 64-bit or equivalent system running Intel Linux, a reliable and efficient internet connection with ample available memory, Collection 5 or Collection 6 MODIS AOD, and Collection 5 or Collection 6 MODIS cloud top property files. The MODIS AOD and cloud top property files must have either an IMAPP or National Aeronautical and Space Administration (NASA) Goddard Space Flight Center (GSFC) naming convention. Once all requirements are met, one can run IDEA-I for any given domain and time period, given that data is available for the domain and time period.

## ***4.2 Running IDEA-I***

IDEA-I first reads in the configuration file supplied by the user. This configuration file feeds IDEA-I the domain bounds, the minimum AOD for trajectory point initialization, the maximum number of trajectory profiles, the option to fetch data files, the output image resolution, and the locations and filenames of the input and output data files. Once IDEA-I reads the configuration file, IDEA-I fetches and reads in the input data files: the GFS meteorological data, the MODIS AOD retrievals, and the MODIS COT retrievals. At this point, IDEA-I is ready to run.

The first action IDEA-I takes after reading in all three input data files is to identify the points in the domain with the highest AOD values. An algorithm within IDEA-I determines where in the domain the retrieved total column AOD is highest. The algorithm then loops, determining the location of the next highest AOD value until either the minimum AOD threshold or the maximum number of trajectory profiles is met. Once all initialization points are determined, IDEA-I sends the coordinates of each initialization point to the LaTM. The LaTM then initializes a set of four trajectories, also known as a trajectory profile, at each set of coordinates. The trajectory profile includes a single trajectory at 50mb above the surface and three more single trajectories at 50mb increments above that. This means that all trajectories are initialized within 200mb of the surface. After initializing each single trajectory, the LaTM then uses the initial point and the GFS meteorology to create trajectories out to 60 hours from model initialization. After the LaTM calculates the path of each trajectory, IDEA-I then creates an image of the MODIS AOD and COT retrievals with the trajectory initialization points. IDEA-I also creates additional images of the initial MODIS AOD retrieval with the horizontal wind barbs and six trajectory points at a time from

each trajectory, which are colored as determined by the pressure of the trajectory point. These images are generated from the first time step to the final time. IDEA-I creates one of these images for each hour within the forecast. IDEA-I also outputs two netCDF data files, one file containing gridded data for the domain and a separate file containing trajectory data for all trajectory points. From these two output data files, we can create the diagnostics presented in the Methods section.

### ***4.3 Assumptions in IDEA-I***

It is important at this time to note that, within IDEA-I, there are two major assumptions. The first assumption is that the AOD value assigned at trajectory initialization does not change throughout the lifetime of the trajectory. The implication of this is that processes that affect aerosol concentrations along the trajectory, such as deposition, sedimentation, and hygroscopic growth and decay are ignored. The other major assumption in IDEA-I is that all AOD is initialized within the lowest 200mb of the atmosphere. This implies that, within IDEA-I, no aerosol exists in the middle or upper atmosphere at trajectory initiation. These two assumptions are important to note when comparing forecasts to observations later in this paper.

## **5. Methods**

In the following section, we will expand on the processes behind our development and validation of IDEA-I aggregated trajectory forecasts. We will be explaining each process in detail in the order in which they were completed, beginning with running IDEA-I, then

outlining the post-processing of the IDEA-I output, and concluding with describing our analysis which utilize aggregated trajectory analysis.

### ***5.1 Optimization Test***

The minimum AOD threshold and the maximum number of trajectory profiles are set such that the runtime for a single IDEA-I run is limited to a reasonable amount of time. When expansive regions of high aerosol are present in the domain, one would expect to see a greater number of points with an AOD greater than the minimum AOD threshold. If only the minimum AOD threshold is set, then IDEA-I may initialize a large number of trajectory profiles, greatly increasing runtime. If only the maximum number of profiles is set, then the inclusion of trajectories with less than desired AOD values will be included. However, if both the minimum AOD threshold and the maximum number of trajectory profiles are set, then the two thresholds act to limit runtime and maintain investigation of only high AOD regions. In order to best minimize the AOD threshold while maximizing the number of trajectory profiles initialized, while also minimizing the run time, we perform runtime optimization tests between these three variables.

The objective of this optimization is to achieve the greatest number of trajectory profiles with the lowest threshold possible in order to achieve a runtime of approximately six hours. We choose a six hour runtime based on real-time application constraints. Included in the six hour time constraint are data retrieval, IDEA-I runtime, and post-processing of the IDEA-I output. A subjective analysis of the trajectory forecasts was done for each of four runs to determine the utility of the result. The first run, which used a maximum number of trajectory profiles equal to 250 and a minimum AOD threshold of 0.25, had little coverage and predicted aerosol transport for only the largest AOD regions. This first run implies that a

greater number of trajectories are needed since the minimum AOD in the forecast is greater than one. As a result, we decided to increase the number of trajectory profiles by an order of magnitude to 2500 and hold the minimum AOD threshold at 0.25 for the second IDEA-I run. With the increase in the number of trajectories, the trajectory forecast images exhibited much greater coverage and structure in the AOD field. However, the runtime for these parameters was close to one day, an unacceptable runtime for a real-time application of IDEA-I. As such, we increase the minimum AOD threshold to 0.75 for our third run, keeping the number of trajectory profiles constant at 2500. Although runtime was significantly improved, the resulting AOD map looked much more like that from the first run, only regional coverage with the very high AOD and the trajectory profile limit was not reached. Consequently, we lowered our AOD threshold for the fourth and final run to 0.6, again keeping the number of trajectory profiles constant at 2500. Although the lowering of the AOD threshold was a modest 0.15 units, the resulting AOD maps exhibited much greater coverage and detail while only running an average of an hour and a half longer than the previous run. The 0.6 unit AOD threshold is also high enough such that much of the observed AOD should be that from wildfire smoke plumes, which are associated with high AODs. With a favorable runtime and AOD threshold, we elect to analyze further the output from the run with an AOD threshold equal to 0.6 and a maximum number of trajectory profiles equal to 2500.

## ***5.2 Post-processing of IDEA-I Output***

Post-processing of IDEA-I output is vital to this study, as without it, we could not forecast which portion of the total AOD column resides within the PBL. In Figure 1, we present a schematic visualizing the pertinent variables output by IDEA-I along with the

calculated variables necessary to determine the forecast AOD that resides within the PBL. The calculated variables are described in this subsection.

### ***5.2.1 Calculating PBL Top Pressure and Trajectory Point Height***

In order to determine how much aerosol in a column is in the PBL, we need to have either both the pressure at the top of the PBL (ppbl) and the pressure coordinate of a trajectory point (ptraj) or both the altitude of the top of the PBL (zpbl) and the altitude of a trajectory point (ztraj). However, IDEA-I only outputs ptraj and the depth of the PBL (hpbl), thus forcing us to compute ppbl and ztraj using the gridded meteorological and IDEA-I trajectory netCDF output files. In order to obtain the ppbl and ztraj variables, we first sum the surface elevation (zsf) and hpbl from the raw IDEA-I gridded data file to obtain zpbl. We then interpolate the height and pressure profiles from the GFS meteorological data file and interpolate the zpbl and ptraj variables to obtain the ppbl and ztraj variables, respectively, for each latitude and longitude point. With both ppbl and ztraj, we are able to perform our analyses in both pressure and altitude coordinates.

### ***5.2.2 Calculating Extinction Coefficient***

Now that we are able to determine whether a trajectory point lies within the PBL, we would like to be able to determine how much aerosol resides in the PBL. The most accurate way to do this with the information provided by IDEA-I is to determine the initial extinction coefficient (exttr) from the initial AOD of the trajectory profile (aodtr). We calculate the extinction coefficient by first determining the depth of the layer, in meters, that each individual trajectory represents. The depth that each layer represents is determined by the 50mb difference in initial trajectory pressure. Once the depths of the individual layers are calculated, we calculate exttr for each individual trajectory by dividing the initial AOD value

by the depth of the corresponding layer ( $dz_x$ ). The assumption that all AOD resides within the PBL influences the initial  $exttr$  value for each trajectory. Figure 1 visualizes the  $exttr$  calculation. For the lifetime of the trajectory, both AOD and extinction coefficient are held constant. This is an unrealistic assumption that would not hold true in Earth's atmosphere due to changes in relative humidity, hygroscopic growth and decay, and emission and deposition processes.

After calculating the pressure at the top of the PBL, the height of each trajectory point, and the initial extinction coefficient, we add these variables to revised IDEA-I gridded and trajectory output files. The revised gridded output file contains the raw IDEA-I gridded data (including  $zpbl$ ,  $hpbl$ ,  $zsfcl$ ) with the addition of the pressure at the top of the PBL ( $ppbl$ ). The revised trajectory data file includes the raw trajectory data (including  $aodtr$  and  $ptraj$ ), the elevation of each trajectory point ( $ztraj$ ), and the initial extinction coefficient ( $exttr$ ).

### ***5.3 Trajectory Aggregation***

The aggregated trajectory maps are the compilation of all valid trajectory forecasts for a given time. The process to create an aggregated trajectory map begins by reading in both the post-processed gridded data file and post-processed trajectory data file. The IDEA-I trajectory aggregation then uses gridded data to create a six dimensional bin array. The six dimensions are satellite, time, latitude, longitude, height, and PBL designation. The satellite dimension refers to whether the data originates from the IDEA-I run initialized using either Aqua MODIS AOD or from the IDEA-I run initialized using Terra MODIS AOD. The time dimension refers to the 18 6-hour time steps present between 12Z on July 16, 2014 and 00Z on July 21, 2014. Both the latitude and longitude bins are  $0.5^\circ$  in size, while the height bin is 50m. Last, the PBL designation refers to whether the trajectory point being binned resides

within the PBL or not. The IDEA-I trajectory aggregation compares the PBL height for each 6-hour period to the heights of each trajectory point to determine whether the trajectory points reside within the PBL or not. Figure 1 also provides a visualization of the trajectory aggregation process in addition to the calculation of  $\text{exttr}$  explained earlier. Once the IDEA-I trajectory aggregation has placed all the trajectory data into the correct bin, we can create maps of the number, mean age, and the mean extinction of all trajectory points in each bin. We also combined the runs initialized with Aqua and Terra into a single combined MODIS analysis. The binned data is the output to a separate data file used in subsequent analysis.

## ***5.4 Diagnostics***

In this section of the paper, we will describe the three diagnostic analyses we develop using the results of trajectory aggregation. We will first discuss the forecast PBL AOD map, then the forecast longitudinal cross-section of extinction, and last, the forecast point profile of extinction

### ***5.4.1 Forecast PBL AOD Map***

The main motivation behind this study is to improve the ability of forecasting surface air quality using satellite data. Although we cannot directly forecast surface  $\text{PM}_{2.5}$  with the variables we have, we can determine how much aerosol resides within the PBL. The forecast PBL AOD map is the portion of the total column AOD forecast to reside within the PBL. This diagnostic allows an air quality forecaster to see where IDEA-I predicts possible surface  $\text{PM}_{2.5}$  enhancement. To create this forecast map, we multiply the mean extinction within the PBL from the trajectory analysis and the PBL height at each point to map the forecast PBL AOD. We directly compare this diagnostic to the retrieved total column AOD image, the True Color RGB image, and the daily average  $\text{PM}_{2.5}$  AQI maps for forecast verification.

#### ***5.4.2 Scatter Plots and Time Series of PBL AOD and PM<sub>2.5</sub>***

We also validate the forecast PBL AOD to the hourly average PM<sub>2.5</sub> data. We create co-located surface PM<sub>2.5</sub> and PBL AOD scatter plots and time series for each site within the domain using a coincidence data file. The coincidence data file contains surface PM<sub>2.5</sub> data for a site and the PBL AOD value for the grid box within which the site resides. In addition to scatter plots for each individual site, a scatter plot is also created for the entire domain by aggregating the data from the coincidence files. A line is included on the scatter plot corresponding to a 60 $\mu\text{m}/\text{m}^3$  increase in PM<sub>2.5</sub> for every 1 unit increase in AOD. Hoff and Christopher (2009) postulate this ratio as a reasonable estimate of the PM<sub>2.5</sub> to AOD ratio, although they also report a wide range of PM<sub>2.5</sub> to AOD ratio estimates among the air quality research community (Hoff and Christopher, 2009). For each site, we also calculate the correlation coefficient of the relationship between PM<sub>2.5</sub> and AOD.

#### ***5.4.3 Forecast Longitudinal Cross Section of Extinction Coefficient***

In order to investigate the forecast of the vertical structure of aerosols in the atmosphere, we create longitudinal cross sections of extinction coefficient every six hours along each integer line of longitude between 140W and 55W, as well as cross sections three and five degrees in width to increase the amount of trajectory data points in each cross section. The cross sections are created using 50m vertical bins that extend from fifty meters below mean sea level to ten kilometers above mean sea level (AMSL) in the vertical from 30°N to 60°N. Each resulting aggregated cross section outputs data into its own output file for the purpose of subsequent analysis. The time of day determines whether the cross section is plotted with north (00Z or 18Z) or south (06Z or 12Z) on the right. This is done to

facilitate easier comparison with the CALIOP lidar data in either an ascending or descending orbit.

#### ***5.4.4 Forecast Extinction Coefficient Point Profile***

One additional diagnostic to assess the air quality forecasting capabilities of IDEA-I is an aggregated trajectory extinction profile forecast. The aggregated trajectory extinction profile forecast utilizes the data obtained from the aggregated trajectory longitudinal cross section at a specified latitude for all forecast times in a given time period. The result of this analysis is a time-height plot of extinction coefficient, which allows for the examination of the vertical structure of aerosols over a single point in the domain for the specified time period. Validation for this diagnostic is performed through comparison with surface-based lidar observations.

In order to create the aggregated trajectory extinction profile forecast, we read in the output from each longitudinal cross-section corresponding with the point of interest and extract from those data sets the data for the latitude of interest. For the case study, we are examining extinction in the column over 40N, 105W, the coordinate in our domain that is nearest the BAO in Erie, Colorado. We choose this latitude-longitude point because of its proximity to the BAO tower. With the available surface-based lidar measurements, direct comparisons are made with the aggregated extinction profile time series.

## **6. Case Study**

To validate the trajectory aggregation diagnostics, we choose to examine a case study for the period starting July 16, 2014 and ending July 20, 2014. For much of June and July of

2014, western North America experienced above (in some cases much above) normal temperatures and very dry weather. Many locations throughout British Columbia, Alberta, the Yukon Territories, and the Northwest Territories recorded less than 1.5 cm of rain over the first half of July (Fort Simpson, Northwest Territory – 12 mm, Baynes Lake Kootenay River, British Columbia – 2 mm, Okotoks, Alberta – 4.8 mm, and Creston, British Columbia – 1.8mm; from [climate.weather.gc.ca](http://climate.weather.gc.ca)). In the Pacific Northwest, similar conditions prevailed (Spokane – 0.13”, Boise, ID – none; from NWS). Many of those same locations had high temperatures averaging two to four degrees Celsius (°C) above the local climatological average. The peak of the early to mid-July heat wave occurred between July 12 and July 16, with many locations recording high temperatures closer to 20 degrees above normal and relative humidity values near 20% or lower. Fort Simpson in the southwestern Northwest Territories recorded a record high temperature of 36.6°C on July 13, 12.9°C higher than the climatological average of 23.7°C ([climate.weather.gc.ca](http://climate.weather.gc.ca)). As this region had seen little precipitation and warm temperatures over the previous two weeks, this five day period of hot and dry weather allowed for the ignition and spread of wildfires. At the end of the heat wave (July 14-July 17), thunderstorms occurred over many locations in Western Canada and the Pacific Northwest, many accompanied by little to no rainfall. With the existing environment, these mostly dry thunderstorms likely would have ignited many wildfires.

The existing dry conditions, heat wave, and dry thunderstorms all aided in setting up a major wildfire outbreak between July 16<sup>th</sup> to July 18<sup>th</sup>, the three day period of greatest biomass burning in the CONUS during the summer of 2014. Figure 2 shows the daily, real-time 1x1 degree Real-time Air Quality Modeling System (RAQMS) biomass burning area estimates following the approach outlined in Al-Saadi et al., (2008). On July 17, 2014, there

were 184 active wildfires in Canada alone

(<http://www.ciffc.ca/firewire/current.php?lang=en&date=20140717p>).

In addition to the active wildfire activity between July 16 and July 18, two air quality field missions were active in the Northern Front Range Metropolitan Area (NFRMA) in central Colorado at the same time, Deriving Information on Surface conditions from COlumn and Vertically Resolved Observations Relevant to Air Quality (DISCOVER-AQ; <http://www-air.larc.nasa.gov/missions/discover-aq/discover-aq.html>) and the Front Range Air Pollution and Photochemistry Experiment (FRAPPE; <https://www2.acom.ucar.edu/frappe>) aimed to better understand many of the issues impacting air quality in the NFRMA. The FRAPPE field mission's focus was understanding the factors and processes governing ground-level ozone in the NFRMA for better model development and more accurate air quality forecasts. The DISCOVER-AQ field mission's focus was on better understanding the relationships between column measurements and surface observations of atmospheric constituents. DISCOVER-AQ also examined how horizontal variability affects satellite measurements and model output. Because the largest active wildfire outbreak in the CONUS for the summer of 2014 was at its peak coincident with the DISCOVER-AQ and FRAPPE field campaigns, we elected to examine the five day stretch from July 16, 2014 to July 20, 2014 with IDEA-I.

## **7. Case Study Results**

One of the objectives of this study is to investigate the accuracy of the aggregated IDEA-I trajectory forecasts in predicting the spatial and temporal distribution of aerosols in

the PBL, principally those from wildfire emissions. The results of this investigation are organized into three different sections. In the first section, we compare MODIS retrieved total column AOD imagery, MODIS RGB imagery, IDEA-I forecast PBL AOD plots, and daily average surface PM<sub>2.5</sub> AQI maps. In the second section, we compare attenuated backscatter CALIPSO lidar images to IDEA-I forecast longitudinal cross sections of extinction coefficient. In the final section, we compare UW-SSEC HSRL lidar observations taken at the BAO tower in Erie, CO to the IDEA-I forecast extinction coefficient profile over the point (40°N, 105°W).

### ***7.1 Comparison of MODIS Imagery, AirNow PM<sub>2.5</sub> AQI, and Forecast PBL AOD Maps***

To compare MODIS AOD, MODIS RGB, IDEA-I forecast PBL AOD, and AirNow surface PM<sub>2.5</sub>, we obtain total column AOD and RGB images from NESDIS, AirNow daily average PM<sub>2.5</sub> AQI images from the AirNow archive, and forecast PBL AOD images using the output from IDEA-I. These four-panel plots are created for each day between July 16, 2014 and July 20, 2014.

#### ***7.1.1 July 16, 2014***

In the AOD image for July 16, 2014 (Figure 3, top left), one can see a large region of very high total column AOD across much of southern and central Canada, extending into the Pacific Northwest. Within this general area of very high AOD, there are a few specific features to note: a region in central British Columbia, a lobe extending from south-central Saskatchewan southwestward into western Montana and northern Idaho, and another lobe extending from northern Manitoba southward across Lake Winnipeg to the Manitoba/North

Dakota border. In addition to the large region of very high AOD, there are also a few small hotspots of enhanced AOD throughout eastern Washington, central Oregon, and southwestern Idaho. In analyzing the MODIS RGB image for this day (Figure 3, top right), one can also find expansive regions of smoke co-located with the large region of very high AOD over much of the western half of Canada. Smoke can also be seen in regions where AOD is not retrieved over northern Alberta, Saskatchewan, and Manitoba. These locations also have regions of cloud cover, which impair the retrieval of AOD. Another interesting feature seen in the RGB image is the smoke plume over British Columbia. A wildfire is likely present over west-central British Columbia with a smoke plume extending southwestward, resulting in the region of high AOD observed over south-central British Columbia. There is also a lack of AOD retrieval near the source of this smoke plume, implying that the dense smoke is mistaken as cloud cover by the AOD retrieval algorithm. There are other regions of dense smoke that are also mistaken as cloud cover, including a small region over north-central Oregon, a small area in far southwestern Alberta, and an east-west oriented linear region in far west-central Alberta.

To examine if and how much observed aerosol is affecting the surface, we next examine the daily average  $PM_{2.5}$  AQI image (Figure 3, bottom right). We can see in this image that unhealthy levels of  $PM_{2.5}$  are observed in central British Columbia, western Alberta, and southwestern Idaho. In each of these regions, active wildfires have been observed. The smoke plume in west-central British Columbia observed in both the AOD and RGB images appears to be affecting the surface. Multiple smoke plumes observed in western Alberta by the AOD image and confirmed by the RGB image are contributing to the poor air quality in that region as well. A wildfire is the likely reason for the poor air quality around

Boise. However, without fire detection data, we can only speculate on this. There are also regions of Unhealthy for Sensitive Groups (USG) air quality observed in Washington, as well as in locations surrounding the Unhealthy AQI regions. These two small regions of USG AQI are also likely related to wildfires in and around these regions

As we look at the 18Z aggregated trajectory forecast PBL AOD for July 16, 2014 (Figure 3, bottom left), one can see a relative lack of coverage compared to the total column AOD retrieval from MODIS. The only regions in western North America forecast to have PBL AOD greater than 0.25 units are over eastern Alberta, Saskatchewan, Manitoba, a small region north of Lake Tahoe, and an even smaller area near the southern Idaho/Montana border. These regions do occur in locations where total column AOD is maximized. However, there are many other locations where no PBL AOD is forecast and high total column AOD is observed. It is in these locations where lofted aerosols reside. Comparing the PBL AOD image to the PM<sub>2.5</sub> AQI image, we can see that, although some PBL AOD is forecast where high PM<sub>2.5</sub> concentrations are observed, there is a lack of observed PM where the greatest PBL AOD is forecast.

### ***7.1.2 July 17, 2014***

One day later, MODIS retrieves aerosol over much of southern Canada, the southern shores of James Bay, and much of the north-central CONUS (Figure 4, top left). One can also find smaller pockets of high total column AOD over southwestern Idaho, eastern Washington, north-central Oregon, and parts of the Rocky Mountains in British Columbia. These smaller features are also observed in the AOD image from the previous day (Figure 3, top left). With the persistence of these features, it is highly likely that these features are active fires. There is also a lack of AOD retrieval in regions in which we might expect to see

very high AOD. These regions include the southwestern shores of Hudson Bay south-southwestward into northern Nebraska, Wisconsin, and southwestern Saskatchewan; eastern British Columbia and Alberta; and much of southern Idaho and Nevada. Looking at the MODIS RGB image for this day (Figure 4, top right), we can see the presence of cloud cover in all these locations as might be expected. One interesting feature in this RGB image is what appears to be the presence of aerosol over cloud cover in western Ontario southward into Minnesota, Wisconsin, northern Illinois, and northern Indiana. This will be investigated further when we examine CALIOP lidar data in the next section.

In the daily average PM<sub>2.5</sub> AQI image for this day (Figure 4, bottom right), one can see Unhealthy air quality due to PM<sub>2.5</sub> in central British Columbia, southwestern Idaho, and central Washington. Comparing this image to the RGB image, we can see a dense smoke plumes co-located with the worst air quality in central British Columbia and central Washington. As for southwestern Idaho, smoke is seen in this region. The cloud cover in the area immediately north and east may also be obscuring the location of the fire as well. We further compare these two images in the USG AQI regions in south-central British Columbia, southwestern Alberta, eastern Oregon, and north-central Washington. The USG regions in south-central British Columbia and north-central Washington are likely the downstream impacts of wildfires. The USG region over eastern Oregon is likely smoke from wildfires over central Oregon. The remaining USG region lies below cloud cover, which precludes us from making any assertions about this feature.

In the forecast PBL AOD image (Figure 4, bottom left), we see PBL AOD greater than 0.2 forecast across much of south-central Canada, portions of the CONUS from southwestern Idaho into far northwestern MN, and a localized region north of Lake Tahoe.

Much of the highest forecast PBL AOD resides to the west of the regions of observed high fine particulate matter. However, there are a few locations where PBL AOD is forecast and  $PM_{2.5}$  are observed. These locations include central British Columbia, southwest Manitoba, and northwestern Nevada north of Lake Tahoe. The forecast PBL AOD map looks more similar to the observed AOD image for this day, with the highest forecast PBL AOD co-located with the largest region of observed total column AOD greater than or equal to one.

### ***7.1.3 July 18, 2014***

On the next day, July 18, 2014, the retrieved total column AOD (Figure 5, top left) appears to be in mainly three separate regions: Quebec, far western Ontario south and south-southwestward into Minnesota, and much of Montana, northern Idaho, and southwestern Alberta. High AOD is also observed over southwestern Idaho; northern Utah; central South Dakota; and central Kansas. There also appears to be many locations where AOD is not retrieved due to the presence of cloud cover or the misinterpretation of dense smoke as cloud, including much of the aerosol plume extending from southeastern Washington into Montana and up into Alberta, much of Saskatchewan and Manitoba, and the Midwest. We can confirm this by looking at the MODIS RGB image (Figure 5, top right) and finding cloud cover in all of these locations. There are also clouds obscuring MODIS's retrieval of AOD over much of British Columbia as well, a region where fire activity has been observed in the previous two days.

Looking at the daily average  $PM_{2.5}$  AQI image (Figure 5, bottom right), one can see a large region of Unhealthy AQI air over much of eastern Oregon, with USG recorded over central British Columbia, northern Idaho and far northwestern Montana into southwestern British Columbia, and central Washington. The surface  $PM_{2.5}$  observations appear to

correlate fairly well with the observed AOD and smoke from the previous two images presented. The Unhealthy region in Oregon is likely the result of wildfires in central Oregon. The central British Columbia region was under cloud cover as MODIS took the image, preventing any analysis of the region. In this case, the only comparison we can make in this region is with the forecast PBL AOD image (Figure 5, bottom left). Here, we see a lack of forecast PBL AOD, which is the result of a lack of AOD retrieval in the region. Elsewhere in the image, we see very high (greater than 0.8) PBL AOD in southern Quebec, eastern Washington, and portions of eastern Montana into southern Alberta and Saskatchewan. These forecasts are slightly further west than the surface  $PM_{2.5}$  measurements would indicate, but are forecasting well in relation to the total AOD column. Absent in the daily average  $PM_{2.5}$  AQI image is the surface reflection of the AOD across Quebec, meaning that nearly all AOD in the column is aloft. Also, absent in the forecast PBL AOD image is any PBL AOD over Oregon, which does not agree with the daily average  $PM_{2.5}$  AQI image.

#### ***7.1.4 July 19, 2014***

The AOD image for July 19, 2014 (Figure 6, top left) shows the retrieval of high total column AOD over the St. Lawrence River valley into the Maine, New Brunswick, and Nova Scotia; from over the southwestern shore of James Bay southwestward towards Lake Superior; over the Dakotas; and over southeastern Colorado. There is also a localized region in north central Oregon showing high AOD. This small region of very high AOD, along with the Unhealthy AQI observed in central Oregon in previous days, likely is the observation of a fire. Cloud cover obscures this feature on July 18, but its existence can be inferred from the feature's persistence. There also appears to be a lack of AOD retrieval over much of western Canada, Washington, northern Idaho, and Montana. One can see in the RGB image (Figure

6, top right) that this is nearly all due to the presence of clouds. The lack of AOD retrieval over western Ontario and the western Great Lakes states is also due to cloud cover, but may also have a dense smoke flagged as cloud component as well. Elsewhere in the RGB image, one can find smoke over and around the state of Nevada, the entirety of James Bay northeastward into Hudson Bay, and possibly over the state of Maine. The smoke over Nevada and Maine also has cloud cover contaminating the retrieval, while the smoke over James and Hudson Bays is not retrieved likely due to differences in the AOD retrieval algorithm over water mistaking the aerosol for cloud cover.

In looking at the daily average  $PM_{2.5}$  AQI image for this day (Figure 6, bottom right), one can find Unhealthy air quality due to  $PM_{2.5}$  in northeastern Washington and central Oregon, with USG observed across western Montana, south-central Oregon, and near Boise, Idaho. Moderate levels of  $PM_{2.5}$  are observed across much of Idaho southeastward into northern Colorado, the Midwestern states, and southern Alberta. The location of the localized very high AOD region in north-central Oregon lies within the region of Unhealthy AQI observed over north-central Oregon. This means that it is likely that the smoke plume from at least one wildfire is observed at the surface. As for the Unhealthy AQI regions over northeastern Washington, little is retrieved from the MODIS satellite due to cloud cover obscuring the surface. The same issue is present when looking at the USG AQI over western Montana and far southeastern British Columbia. As for the USG AQI regions over south-central Oregon and Boise, Idaho, cloud cover does not obscure these locations. In the RGB image, there does appear to be smoke present in the region. Evidence for this claim can be seen in the AOD retrieval image, with AOD of  $\sim 0.5$  units observed from northwestern Nevada into southern Idaho.

The PBL AOD forecast for this day (Figure 6, bottom left) shows a large region of PBL AOD greater than 1 across much of eastern Montana, southern Saskatchewan, and southwestern Alberta. There are also smaller pockets of intense PBL AOD over southwestern Minnesota, southwest of James Bay, portions of Quebec and Labrador, and portions of eastern Manitoba. Many of these features are not found in the surface PM<sub>2.5</sub> measurements. However, there are a few features forecast across the domain, such as the southeastern Manitoba and St. Lawrence River valley features, that have corresponding Moderate AQI features in the daily average PM<sub>2.5</sub> AQI image.

#### ***7.1.5 July 20, 2014***

For this day, much of the AOD retrieval for July 20, 2014 (Figure 7, top left) is not present. The only portions of the AOD retrieval present are over Canada, northern North Dakota, and the Pacific Coast states. The only high AOD retrieved on this day was over northern Alberta and Manitoba, the mouth of the St. Lawrence River, and southern Canada just across the border from Montana. A more complete picture comes through when looking at the RGB image for this day (Figure 7, top right). Cloud cover is present over much of Canada, the eastern CONUS, and portions of the intermountain west. Smoke is likely seen across the Mississippi River valley, Quebec, and northern portions of Alberta and Saskatchewan. However, clouds are also present across each of these locations, which would make the retrieval of pertinent AOD difficult even without any other issues.

In the daily average PM<sub>2.5</sub> AQI image (Figure 7, bottom right), high PM<sub>2.5</sub> is observed across southwestern Manitoba, near Boise, Idaho, and across much of the Midwest. Manitoba and Boise are under cloud cover, so little can be said about the direct cause of the PM<sub>2.5</sub> enhancement at these locations. However, smoke does appear to be present across much of

the region reporting Moderate daily average  $PM_{2.5}$  AQI over the Midwest. If this is the case, then the implication is that smoke is affecting the surface. This could be the same smoke emitted by wildfire smoke plumes, lofted days earlier subsiding to the surface.

The forecast PBL AOD for this day (Figure 7, bottom left) shows large values along the northern CONUS and southern Canadian border, western Ontario, southeastern Montana, New Brunswick, and Quebec. Comparing this to the surface  $PM_{2.5}$  observations, there is agreement in the location of the forecast PBL AOD. The Moderate  $PM_{2.5}$  region between Salt Lake City, UT and Brandon, Manitoba closely resembles the shape of the forecast region from eastern North Dakota to Billings, Montana and Cheyenne, WY. Moderate PBL AOD is forecast across the western Great Lakes, only slightly displaced westward from the observed Moderate AQI region in the Midwest.

## ***7.2 Correlation Between Observed $PM_{2.5}$ and Forecast PBL AOD***

With both the observed surface  $PM_{2.5}$  and the forecast PBL AOD data sets, we are able to investigate a P/A relationship for the PBL. We map the calculated P/A ratio, the  $PM_{2.5}$  time series, and the AOD time series for each  $PM_{2.5}$  monitor within the domain. However, we do not show these results. The results for the calculated P/A ratio span many orders of magnitude, which make the portrayal of the results confounding. As for the correlation coefficients for each site, we do show this map in Figure 8. We only plot sites with three or more coincidences of forecast PBL AOD and valid  $PM_{2.5}$  observations. One can see from looking at Figure 8 that correlation coefficients tend to be modestly to strongly positive across the Great Lakes region, while modest to strong negative correlations are observed across the Rocky Mountain states and provinces. In northern Canada, central Canada, the Dakotas, and western Minnesota, correlations are quite weak. Across the northeastern

CONUS and eastern Canada, correlations show little coherence amongst one another. We would also like to point out the positive correlation at a few locations in eastern Washington. These are of significance as there were active wildfires very near these locations. This suggests that the smoke plumes from these wildfires remained in the PBL from the true location of the fires. Coupling this with the negative correlations over much of the rest of the Rocky Mountains, the weak correlation over central North America, and the positive correlations over the Great Lakes suggests the smoke plumes from wildfires burning in the Pacific Northwest loft aerosol above the PBL over Alberta, Idaho, and Utah. The lofted aerosol then begins to descend into the PBL across Saskatchewan, Manitoba, Montana, North Dakota, and western Minnesota, with the bulk of the aerosols descending once they reach eastern Minnesota, Iowa, and Wisconsin.

### ***7.3 CALIOP Vertical Feature Mask Images vs. IDEA-I Longitudinal Cross-Sections of Extinction Coefficient***

In this section, we will be comparing the vertical feature mask images taken by CALIOP to the longitudinal cross-sections of extinction coefficient from IDEA-I aggregated forecasts. We will be examining the daytime CALIPSO overpasses of North America, as these images most closely correspond temporally to the Aqua MODIS imagery and the forecast PBL AOD maps presented in Figures 3-7. We will also be examining five degree wide longitudinal cross-sections of extinction coefficient created using the IDEA-I aggregated forecasts. For each day, we examine the vertical feature mask image for the daytime CALIPSO overpass of North America for which the most data is available in the corresponding longitudinal cross-section.

### ***7.3.1 July 16, 2014***

The CALIPSO overpass on July 16, 2014 that we analyze occurred just before 21Z. This overpass stretches from far north-central Mexico across the CONUS and Canada into the Beaufort Sea (Figure 9). The CALIOP vertical feature mask image for this overpass (Figure 10) shows numerous aerosol features across the United States and Canada. These features include three surface aerosol layers: one over the Canadian Rockies into central Alberta (A), a second over northern Montana (B), and a third surface aerosol layer over Utah (C). A lofted aerosol layer is also observed over Idaho and Montana (D). The features over Idaho and Montana, as well as the feature over Alberta, are easily seen in the AOD and RGB imaged for this day. However, the feature over central Utah is not. If we look at the 115W-120W extinction coefficient cross-section for 18Z on this day (Figure 11), we can see aerosol forecast between 50°N and 58°N, between 45°N and 50°N, and at 40°N. Each of these three features has an analog in the CALIOP vertical feature image. The feature forecast between 50°N and 58°N is in nearly the same location as feature A. This feature also has a very similar shape and vertical extent as feature A. As such, we mark this feature in the extinction cross-section with an A as well to denote that they are the same feature. The feature between 45°N and 50°N closely corresponds to feature B in the vertical feature mask image. The observations only have the feature extending as far south as 47°N, but both the forecast and observed features extend up to about 4 kilometers and span the region between 47°N and 50°N. As there is much agreement in the two features, we can label this feature with a B, signifying that they are likely the same feature. As for the features in the vertical feature mask labelled C and D, these two features are observed too far south of the latitude range of

the forecast cross-section valid for the CALIPSO track. Any speculations made concerning either of these features are just that: speculation. One speculation we make is that feature C may have a corresponding feature in the forecast image. An aerosol layer is forecast between 2 kilometers AMSL and 4 kilometers AMSL at 40°N, which is near the same latitude as feature C. With the accurate forecast of two observed features, and possibly a third, we can say that IDEA-I was able to forecast well for this day, despite not forecasting the observed lofted feature between 46°N and 47.5°N.

### **7.3.2 July 17, 2014**

The CALIPSO overpass of North America on July 17, 2014 that we analyze occurred just before 20Z. This overpass extends from the Gulf of Mexico just offshore of Houston, TX to the far eastern Beaufort Sea (Figure 12). The CALIOP vertical feature mask image for this overpass (Figure 13) has two aerosol features of interest. The first is a layer from the surface to 3 kilometers AMSL around 53°N (A). The other is an aerosol and cloud layer that descends from 6.5 kilometers AMSL over 47°N to the top of the first feature (B). The 18Z 100W-105W extinction coefficient cross-section for this day (Figure 14) forecasts high aerosol between 50°N and 54°N, with the highest concentrations around 3 kilometers AMSL (A). This feature is in the same location as the surface aerosol feature from Figure 13, which is why we label this feature with an 'A' as well. However, the lofted feature in the CALIOP vertical feature mask image (feature 'B') is not forecast by IDEA-I. As such, there is no feature labelled with a 'B' in Figure 14. Overall, IDEA-I forecast modestly for this day. Although IDEA-I forecast observed feature A quite well, it did not forecast the observed lofted aerosol layer at all. In addition to not forecasting an observed feature, IDEA-I also forecast a 2.5 kilometer deep aerosol layer between 40°N and 50°N that did not verify.

### ***7.3.3 July 18, 2014***

The CALIPSO overpass of North America on July 18, 2014 that we analyze occurred around 19Z, observing a path from central Florida across the Great Lakes and into the Canadian Arctic Archipelago (Figure 15). The CALIOP vertical feature mask image for this day (Figure 16) shows an aerosol layer over Lake Superior and western Ontario (A). This aerosol layer over Lake Superior initially appears at 11 kilometers AMSL, which is outside the domain of the IDEA-I forecast image. However, the layer descends to 4 kilometers as one moves over western Ontario. In the forecast extinction coefficient cross-section from IDEA-I (Figure 17), one can see high extinction coefficients forecast between 52°N and 57°N at an altitude of 3 to 4.5 kilometers AMSL. North of 55°N, IDEA-I forecasts aerosol from the surface up to 10 kilometers. This forecast verifies for the portion of the observed aerosol layer over western Ontario and thus we label this region with an A. However, IDEA-I also forecasts more aerosol than observed, and the descending portion of this aerosol layer is not forecast well at all. In addition to not forecasting half of the observed aerosol layer, both aerosol forecasts from the surface to 10 kilometers AMSL and the aerosol forecast up to 3 kilometers AMSL between 43°N and 50°N do not verify. Neither forecast feature appears at all in the CALIOP vertical feature mask image. Although IDEA-I forecast observed feature A quite well, the rest of the forecast was not very good.

### ***7.3.4 July 19, 2014***

The CALIPSO overpass of North America on July 19, 2014 that we analyze occurred around 19Z, observing along a path from just south of the Louisiana coast through the central

CONUS and Canada to the westernmost portions of the Canadian Arctic Archipelago (Figure 18). In the CALIOP vertical feature mask image recorded during this overpass (Figure 19), one can find two expansive and lofted aerosol layers. One aerosol layer at 5 kilometers AMSL from southwestern Minnesota to the northern end of Lake Winnipeg in central Manitoba (A) while the other is over the southeastern CONUS between 4 and 8 kilometers AMSL (B). In the IDEA-I extinction coefficient forecast image (Figure 20), one can find strong aerosol enhancement at around 4 kilometers AMSL at 45°N, which then descends to just below 3 kilometers AMSL. There is also strong aerosol enhancement below this feature between 44°N and 45°N, with moderate enhancement elsewhere below this layer. As the forecast feature has many similar characteristics to observed feature A, we label this forecast concentrated aerosol feature with an A. The feature over the southeastern CONUS is outside the domain of the forecast, so we will not be speculating on forecasts for that feature. IDEA-I forecast this day very well. The most intense aerosol layer (A) observed by CALIOP is not only forecast by IDEA-I in nearly the identical location as is observed, the forecast also captures the one kilometer descent of the aerosol layer. The only issue IDEA-I had in forecasting for this day was the forecast of surface aerosol enhancement that did not verify. Although there was a little over-prediction of aerosols, the ability with which IDEA-I forecast the observed aerosol feature A allows us to reiterate the fact that IDEA-I forecast very well for this day.

### ***7.3.5 July 20, 2014***

The CALIPSO overpass of North America on July 20, 2014 that we analyze occurred around 1845Z, observing along a path from just east of Florida, through the Carolinas and Great Lakes, and ending over the central portions of the Canadian Arctic Archipelago (Figure

21). In the CALIOP vertical feature mask image for this day (Figure 22), a surface aerosol feature is observed between 49°N and 52°N (A) and a lofted aerosol layer appears between 5 and 8 kilometers AMSL over the eastern CONUS into Ontario (B). In the forecast extinction coefficient cross-section from IDEA-I (Figure 23), we find a forecast of high extinction coefficient about 2.5 kilometers at 48°N and 53°N with general enhancement below 3 kilometers AMSL between 45°N and 52°N. These two regions of higher extinction coefficients provide evidence for the observed aerosol layer seen in CALIOP. However, this feature is forecast too low if this is the case. The feature in the forecast more similar in terms of vertical placement to the cloud feature below the lofted aerosol layer, which is forecast at around 2.5 kilometers AMSL. This cloud layer also happens to coincide with the top of the observed surface aerosol layer. The surface aerosol layer also happens to coincide with the general enhancement feature forecast below 2.5 kilometers AMSL. With this, we decide to label the portion of the general enhancement feature nearest the observed feature with an A. One can observe the lofted aerosol layer above the cloud layer across central Ontario in the RGB image. As such, we make the assertion that the forecast of the aerosol feature is too low. In addition to this feature, general boundary layer aerosol enhancement is forecast north of 41°N. One can then look at the CALIOP vertical feature mask image and find aerosol enhancement within the boundary layer over the northern portions of Lake Huron, which verifies this portion of the IDEA-I forecast. For this day, IDEA-I forecasts well, other than the incorrect placement in the vertical for the aerosol layer.

#### ***7.4 HSRL lidar Observations vs. Forecast Extinction Coefficient Profile***

Our goal with this section is to validate the IDEA-I forecast using the UW-SSEC HSRL lidar profiles. In order to do so, we create the aggregated extinction coefficient profile

over ( $40^{\circ}\text{N}$ ,  $105^{\circ}\text{W}$ ), the approximate coordinates of the BAO tower. The data used in this analysis is extracted from the  $105^{\circ}\text{W}$  longitudinal cross section for each analysis time, or every six hours between 12Z July 16, 2014 – 18Z July 20, 2014 inclusive. The result is a time-height plot of extinction coefficient for the BAO tower.

As part of the FRAPPE field mission, UW's SSEC employed their HSRL to the BAO tower in Erie, CO. Figure 24 presents the lidar profile time series recorded by the UW-HSRL at the BAO tower between 00Z July 16, 2014 and 00Z July 21, 2014. One can pick out many features in the lidar time series. These features include scattered shower activity and cloud cover on July 16 and July 17, a set of three descending aerosol layers above 6 kilometers late on July 17 into July 18, and a deep layer of enhanced aerosol below 6 kilometers AMSL from just after 12Z on July 18 to about 00Z on July 20. The lidar profile time series will be described further in the next paragraph.

Throughout much of the day on July 16 and July 17, the UW-SSEC HSRL observes scattered showers and cloud cover. These features manifest as regions lacking backscatter (black) above a region with high backscatter (red) as the lidar beam attenuates while travelling through the rainfall and parent cloud. One can see some aerosol enhancement near the surface and aloft at near 6 kilometers AMSL through the breaks between in the cloud cover. However, with the intermittency of the data, one should limit any assertions made about the observed aerosol during this time.

After the shower activity and cloud cover subside, three descending lofted aerosol layers appear after 12Z on July 17. The highest layer, which descends from higher than 10 kilometers AMSL, disappears before 00Z on July 18 at around 8.75 kilometers AMSL. The second highest layer also appears around 12Z on July 17, but at an altitude around 9

kilometers AMSL. This feature then descends to 7 kilometers AMSL just after 00Z on July 18 and disappears after rising slightly to 7.5 kilometers AMSL. The third and final descending lofted aerosol feature appears closer to 18Z on July 17 at 6 kilometers AMSL, descends to 6 kilometers AMSL by 06Z on July 18, then disappears after rising to 6.5 kilometers AMSL approximately two hours later.

As for the boundary/residual layer feature seen after 12Z on July 18, one can find aerosols aloft between 4.5 and 6 kilometers AMSL at 12Z. Within a few hours, the aerosol appears to mix down to the surface. Given that the aerosol becomes well mixed so quickly, especially in the presence of upward vertical motion implied by the shower activity near this time, the true cause of the deep aerosol layer may be advection. Aside from some cloud cover above 5 kilometers AMSL late on July 18 and one or two passing clouds very late on July 19, no cloud cover is observed for the rest of the period. This lack of cloud cover and precipitation allows the lidar to monitor this enhanced aerosol layer without issue. For the entirety of July 19, this layer from the surface to approximately 6 kilometers AMSL exhibits a high amount of aerosol. Given that this layer is present for longer than a day, this layer is likely a boundary layer that forms on July 18 after 18Z with a deep residual layer that persists for close to 30 hours. Then, just before 00Z on July 20, the amount of aerosol in this layer decreases greatly, with the backscatter decreasing by an order of magnitude in a 12 hour span.

The IDEA-I forecast extinction profile at (40°N, 105°W; Figure 25) predicts an aerosol layer between 3.5 and 6 kilometers AMSL at 12Z on July 18, below 2.5 kilometers AMSL between 12Z and 18Z on July 19, and aloft between 06Z July 19 and 18Z on July 20. Comparing Figures 24 and 25, we can see that IDEA-I appears to forecast the deep surface

aerosol layer quite well. The initial appearance of the trajectories at 12Z on July 18 coincides with the initiation of the deep surface aerosol layer. The layer is not forecast well between 18Z on July 18 and 06Z on July 19. However, the forecast aerosol present throughout the surface to 5.5 kilometer AMSL layer is in accordance with the aerosol layer after 12Z on July 19. Since aerosol is observed where IDEA-I forecasts, we assert there is validity to the aerosol forecast. However, the lofted aerosol layers observed between 12Z on July 7 and 06Z on July 18 are not forecast at all. We can relate this to the fact that the BAO is on the fringe of the AOD forecast from IDEA-I.

Analyzing the forecast BAO tower profile from IDEA-I, one can see that no aerosol is forecast for the first 42 hours of the profile. However, at 12Z on July 18, 2014, an aerosol layer is forecast over the BAO tower between 3.25 km and 6 km altitude. This aerosol layer is more dense in the lowest kilometer of the layer. Over the next 24 hours, the aerosol layer appears to disperse, as there are no aerosols seen at 00Z on July 19. The aerosol layer reappears at 12Z on July 19 with many of the same characteristics as the aerosol layer observed 24 hours previous. Some of those similarities include a depth of approximately 3 km, extending from 2 km to 5 km, the densest portion of the layer in the lowest regions of the layers, and the magnitude of the upper portion of the aerosol layer. There is also a possible explanation for the lack of continuity in the predicted aggregated extinction profile: trajectories are only initialized every 24 hours. With the intermittency of trajectory initialization, the result over a single location will be an ephemeral realization of the aerosol associated with the trajectory. This means that for any 6 hour period, aerosols at a given location could be quite high, whereas the next 6 hour period may see little to no aerosols as the trajectory has already passed by the region of interest.

By 18Z on July 19, 2014, the forecast aerosol layer has descended to the surface, bringing a great deal of aerosols into the PBL. Six hours later (00Z on July 20), the high extinction values in the lower portion of the aerosol layer are no longer present, while the aerosols in the upper portion of the layer have dispersed in the vertical, increasing in depth from 2 to 3 kilometers. As we move forward another 6 hours to 06Z on July 20, only a portion of the layer around 4 kilometers AMSL is still forecast. This feature at 4 km is then seen throughout the rest of the forecast profile. The aerosol layer returns to the forecast at the end of this profile, albeit much less deep (~1 kilometer in depth) than the layer observed at 12Z on July 19.

Comparing the IDEA-I extinction profile and the UW-HSRL backscatter profile, the feature forecast by IDEA-I for 12Z on July 18 appears to match up well with the HSRL observations from closer to 00Z. As for the observed features at 12Z and 18Z on July 19, there is agreement with the forecast of a possible aerosol layer up to 5 km, as observations have an aerosol layer up to 5.5 km. As for the features from 06Z – 18Z, the forecast has the aerosol layer a kilometer lower than observed by the HSRL. The forecast aerosol layer does not affect the surface either. However, IDEA-I might be hinting some enhancement just below the entrainment zone between the free troposphere and PBL, with the entrainment zone reaching as low as 4.5 km at some points in time.

## **8. Discussion**

Comparison between aggregated aerosol forecasts obtained from IDEA-I output with surface and satellite observations has allowed us to investigate the utility of IDEA-I as a

wildfire smoke plume forecast tool. Other studies have shown that IDEA-I is an effective visualization tool, but may not necessarily aid in the development of quantitative forecasts (Al-Saadi et al., 2005). Our results show that, qualitatively, IDEA-I generally has good utility in forecasting air quality through our comparisons with both MODIS and CALIOP.

However, quantitative results, such as the calculated forecast PBL AOD to observed  $PM_{2.5}$  ratio, exhibit lesser agreement with surface  $PM_{2.5}$  observations. We also find that the PBL AOD forecast helps to better understand the vertical distribution of aerosols in the atmosphere and how that affects surface air quality.

As for the observed features that are not forecast by IDEA-I, multiple explanations exist for the lack of quantitative predictive skill in IDEA-I. These possible explanations include the  $0.5^\circ \times 0.5^\circ$  spatial resolution and 6 hour temporal resolution in the GFS meteorology, the uncertainty in the vertical distribution of aerosols, the assumption that extinction coefficient remains constant along a trajectory, and the restriction of all aerosols present to have been initialized within the lowest 200mb of the atmosphere. These reasons are also explanations for the incorrect forecast of features which never appear.

## ***8.1 Spatial and Temporal Resolution of Input Data Sets***

### ***8.1.1 Meteorology***

To address any issues related to the spatial resolution of the GFS input data, one could use the  $0.25^\circ$  gridded GFS product, available for download from the NCEP FTP site [<ftp://ftp.ncep.noaa.gov/pub/data/nccf/com/gfs/prod/>]. However, the GFS is run only four times a day, which will not improve the temporal resolution of the input data. One remedy to this might be to utilize the Rapid Refresh (RAP) model zero hour output [<ftp://nomads.ncdc.noaa.gov/RUC/13km/>]. The RAP is run hourly on a 13 km grid, making

the RAP a better option in terms of spatial and temporal resolution than the GFS. The only drawback to using the RAP only forecasts for 18 hours. However, since we currently use only the zero hour forecast GFS meteorology, using the zero hour forecast RAP meteorology for each hour would work just as well. At this improved resolution with little drawback, IDEA-I should be able to forecast more features observed by MODIS using the RAP meteorology than it currently does using the GFS meteorology.

### ***8.1.2 Aerosol Optical Depth***

In addition to increasing the temporal and spatial resolution of the meteorology used, increasing the temporal resolution of AOD retrievals will soon be possible with the launch of the GOES-R satellite. GOES-R is scheduled to be launched on October 13, 2016 at 21:43 UTC from Cape Canaveral [<http://www.goes-r.gov/>]. Aboard GOES-R will be the Advanced Baseline Imager (ABI) instrument. The ABI will have the ability to relay hourly to sub-hourly AOD measurements at a spatial resolution of approximately 2 kilometers (<http://www.goes-r.gov/spacesegment/abi.html>). Use of this product will surely improve IDEA-I aerosol forecasts, especially if used in conjunction with greater spatial and temporal resolution meteorology.

## ***8.2 Inclusion of Fire Products***

Currently, IDEA-I is initialized using a trajectory profile at the coordinates with the highest AOD as observed by MODIS instruments. However, in terms of specifically forecasting wildfire smoke plumes, the trajectory initialization scheme can be improved with the inclusion of wildfire location and injection height. Satellites have the capability to locate wildfires (Kaufman et al., 1998; Justice et al., 2002), the coordinates of which could then be used as the location for trajectory profile initialization. The MODIS AOD retrievals would

then be used in determining the initial AOD and extinction coefficient for all trajectory profiles. In addition to a wildfire location product, a wildfire plume injection height would also be useful. Soja et al. (2012) have investigated biomass burning injection height through comparisons between CALIPSO, MODIS, and the LaTM. As Soja et al. (2012) did in their paper, IDEA-I could use the Terra and Aqua MODIS Thermal Anomalies/Fire product (MOD14/MYD14) to determine the location of trajectory profile initialization. The inclusion of biomass burning injection height would allow for a truer representation of the smoke plume in IDEA-I. IDEA-I could use this value in two ways - either as the only level at which a trajectory would be initialized, or as the upper limit of a trajectory profile which would start at the surface.

### ***8.3 Inclusion of Physical Processes***

There are some innate assumptions in IDEA-I that have already been presented in earlier in this paper. These assumptions need to be addressed, as they affect the results quite dramatically. The first improvement to be made to IDEA-I would be the inclusion of a wet deposition and sedimentation scheme. To add accurate emissions into IDEA-I, the Air Resource Laboratory's (ARL) HYSPLIT model operationally forecasts smoke and dust, which are available from the National Weather Service (NWS) (Stein et al., 2015). Knowing that the HYSPLIT model already forecasts aerosol emissions, IDEA-I could use output from the HYSPLIT model to better forecast surface AQ. The other assumption stated previously would be addressed with the inclusion of fire detection and smoke plume injection height products. IDEA-I could just use the coordinates of fires to initialize trajectories in the LaTM and release smoke up to the injection height. The initial aerosol would be different for different, with more aerosol associated with trajectories initiated closer to the injection

height. This would be much more realistic than the existing partitioning of aerosol with height in IDEA-I

#### ***8.4 Aerosol Homogeneity***

Another assumption in IDEA-I is that all AOD is homogeneous. Only AOD is provided to IDEA-I from Aqua and Terra. There is no information on the makeup of the observed aerosols. This lack of aerosol partitioning may lead to the inclusion of aerosols that do not originate in smoke plumes from wildfires. This would mean that aerosols from other sources, including dust, sea salt, and anthropogenic aerosols, are included in IDEA-I along with the aerosol source of importance for this study, wildfire smoke. This is not as much of an issue if one wishes to use IDEA-I to examine total aerosol. However, to examine the contribution of aerosols solely from biomass burning, this could pose an issue. There is little remedy for this issue when wishing to examine solely the contributions from biomass burning; only minimizing the contributions of other aerosol types by initializing trajectories over observed wildfires or, perhaps, using the Ångström exponent to attempt partitioning of certain aerosol types.

#### ***8.5 Retrieval Restriction Due to Cloud Cover***

One inherent issue using MODIS is the restriction of AOD retrieval validity in and around regions of cloudiness throughout the domain, whether the cloud cover is pyrocumulus, fair weather cumulus, upper level cirrus, or even a very thick wildfire smoke plume. This cloud cover restriction does not allow for AOD retrieval at or around the cloudy region, which may prevent the initialization of trajectories in a region of high AOD, especially in close proximity to a wildfire. At this time, little can be done to remedy this issue, as MODIS cannot retrieve AOD in regions of cloudiness. The final issue affecting

IDEA-I that is the lack of any transport into the domain from outside the domain. The domain can always be expanded to include a larger area. However, IDEA-I can only forecast using what already exists within the domain, as all trajectories are initialized within the domain.

### ***8.6 The PM<sub>2.5</sub>/AOD Ratio***

The variance in the P/A ratio for the entire domain is partly the result of a lack of data coincidences and the use of PBL AOD. The total number of trajectory points coincident in time and space with surface PM<sub>2.5</sub> monitors is far fewer than needed to make any assertion with confidence. Many of the surface PM<sub>2.5</sub> monitors have two or fewer coincidences with the forecast PBL AOD. In addition to the lack of coincidences, the P/A ratio at individual locations can vary greatly. The inclusion of such a large variance of P/A ratios will cause the domain-wide P/A ratio to have great uncertainty. We must also remember that in calculating the P/A ratio, we use forecast PBL AOD, not the observed total column AOD. The most important implication of the lack of correlation in the P/A ratio is the lofting of aerosols by wildfires. If the smoke from these plumes is lofted high enough, then neither the surface PM<sub>2.5</sub> monitors observe the smoke nor do the PBL AOD forecasts predict smoke. This may account for some of the lack of PBL AOD in locations downstream of active fires. Although the air quality monitoring and forecasting community has made great strides forward in utilizing satellite data, issues remain in using satellite-based observations to observe and forecast air quality.

## 9. Conclusion

The main point to take away from this study is that IDEA-I can be used as a wildfire smoke plume forecast tool, but should not be the only source of information for making air quality forecasts. Although IDEA-I can accurately predict the locations of highest PBL AOD and provide a reasonably accurate forecast of aerosol in the vertical dimension, the magnitudes of PBL AOD forecasts from IDEA-I need improvement to become usable in air quantitative quality forecast applications. However, IDEA-I can be an important tool in the forecasting of aerosol distribution in the vertical, as the vertical distribution of aerosols is extremely difficult to determine solely from AOD measurements. The vertical distribution of aerosols can better be determined with CALIOP lidar data; however, CALIOP only makes nadir observations. This lack of coverage for any one time severely limits the utility of CALIOP as a forecast option as well. As such, IDEA-I becomes an attractive option for the prediction of aerosols in the vertical.

IDEA-I can be improved with the inclusion of a higher resolution meteorological data set, a wildfire detection product, and a wildfire smoke plume injection height product. The inclusion of these three data sets would result in a more accurate PBL AOD forecast from IDEA-I.

## 10. Future Work

Future work should include implementing the proposed changes, such as adding the ability to initialize trajectory profiles at locations of detected wildfires and to initialize a trajectory at

the plume injection height. With greater data resolution, a more accurate placement of trajectories in relation to active wildfires, and the inclusion of injection height, the ability of IDEA-I to produce more accurate forecasts, especially in the vertical, would likely increase greatly. As the spatial and temporal variability of aerosols can be quite high, the improvements in resolution would allow more structure to be captured and accurately forecast in IDEA-I. The inclusion of wildfire locations and injection heights would allow for more precise initialization of trajectories, which, in turn, would allow for a more accurate forecast of trajectory path. Other further work could include examining incorrect trajectory aggregation forecasts, implementation of a deposition and modeled emission scheme and the initialization of trajectories more than once a day. Analyzing false forecasts could be important in determining whether the initialization for groups of trajectories was incorrect. Also, in terms of air quality forecasting, a busted forecast is almost as bad as not forecasting an air quality event. Many false forecasts could lead to complacency from the public, which could lead to more exposure for true forecasts. A deposition and modeled emission scheme would allow for improvement of the quantitative forecasts from IDEA-I by including physical processes not currently included in IDEA-I. The ability to initialize trajectories every couple of hours, as opposed to once a day, would allow for continuous emission of wildfire smoke. The inclusion of AOD retrievals from GOES-R ABI will have much greater temporal frequency than the current MODIS retrievals. The accurate modeling of continuous wildfire emission would enhance the diagnostics introduced by this study. With the implementation of the proposed changes, IDEA-I would certainly become a more effective aerosol forecasting tool.

## References

- Al-Saadi, J., et al., 2005: Improving national air quality forecasts with satellite aerosol observations. *Bulletin of the American Meteorological Society*, 86, 1249-1261, doi:10.1175/BAMS-86-9-1249.
- Al-Saadi, J., et al., 2008: Intercomparison of near-real-time biomass burning emissions estimates constrained by satellite fire data. *Journal of Applied Remote Sensing*, 2, doi:10.1117/1.2948785.
- Anderson, T. L., Y. Wu, D. A. Chu, B. Schmid, J. Redemann, and O. Dubovik, 2005: Testing the MODIS satellite retrieval of aerosol fine-mode fraction. *Journal of Geophysical Research*, 110, doi:10.1029/2005JD005978.
- Barnes, W. L., T. S. Pagano, and V. V. Salomonson, 1998: Prelaunch characteristics of the Moderate Resolution Imaging Spectrometer (MODIS) on EOS-AM1. *IEEE Transactions on Geoscience and Remote Sensing*, 36 (4), 1088-1100.
- Chu, D. A., Y. J. Kaufman, C. Ichoku, L. A. Remer, D. Tanrè, and B. N. Holben, 2002: Validation of MODIS aerosol optical depth retrieval over land. *Geophysical Research Letters*, 29 (12), doi:10.1029/2001GL013205.
- Diner, D. J., et al., 1998: Multi-angle Imaging SpectroRadiometer (MISR) instrument description and experiment overview. *IEEE Transactions on Geoscience and Remote Sensing*, 36 (4), 1072-1087.
- Duncan, B. N., et al., 2014: Satellite data of atmospheric pollution for U.S. air quality applications: Examples of applications, summary of data end-user resources, answers to FAQs, and common mistakes to avoid. *Atmospheric Environment*, 94, 647-662, doi:10.1016/j.atmosenv.2014.05.061.
- Engel-Cox, J. A., C. H. Holloman, B. W. Coutant, and R. M. Hoff, 2004: Qualitative and quantitative analysis of MODIS satellite sensor data for regional and urban scale air quality. *Atmospheric Environment*, 38, 2495-2509, doi:10.1016/j.atmosenv.2004.01.039.
- Engel-Cox, J. A., et al., 2006: Integrating lidar and satellite optical depth with ambient monitoring for 3-dimensional particulate characterization. *Atmospheric Environment*, 40, 8056-8067, doi:10.1016/j.atmosenv.2006.02.039.
- Esaías, W. E., et al., 1998: An overview of MODIS capabilities for ocean science observations. *IEEE Transactions on Geoscience and Remote Sensing*, 36 (4), 1250-1267.
- Fairlie, T. D., J.-P. Vernier, M. Natarajan, and K. M. Bedka, 2014: Dispersion of the Nabro volcanic plume and its relation to the Asian summer monsoon. *Atmospheric Chemistry and Physics*, 14, 7045-7057, doi:10.5194/acp-14-7045-2014.
- Fairlie, T. D., et al., 2009: Lagrangian sampling of 3-D air quality model results for regional transport contributions to sulfate aerosol concentrations at Baltimore, MD, in summer 2004. *Atmospheric Environment*, 43 (20), 3275-3288, doi:10.1016/j.atmosenv.2009.02.026.
- Fraser, R. S., Y. J. Kaufman, and R. L. Mahoney, 1984: Satellite measurements of aerosol mass and transport. *Atmospheric Environment*, 18 (12), 2577-2584.
- Grund, C. J. and E. W. Eloranta, 1991: The University of Wisconsin High Spectral Resolution Lidar. *Optical Engineering*, 30 (1), 6-12, doi:10.1117/12.55766.
- Gupta, P. and S. A. Christopher, 2008: Seven year particulate matter air quality assessment from surface and satellite measurements. *Atmospheric Chemistry and Physics*, 8, 3311-3324, doi:10.5194/acp-8-3311-2008.

- Gupta, P. and S. A. Christopher, 2009a: Particulate matter air quality assessment using integrated surface, satellite, and meteorological products: 2. A neural network approach. *Journal of Geophysical Research*, 114, D20 205, doi:10.1029/2008JD011497.
- Gupta, P. and S. A. Christopher, 2009b: Particulate matter air quality assessment using integrated surface, satellite, and meteorological products: Multiple regression approach. *Journal of Geophysical Research*, 114, D14 205, doi:10.1029/2008JD011496.
- Herman, J. R., P. K. Bhartia, O. Torres, C. Hsu, C. Seftor, and E. Celarier, 1997: Global distribution of UV-absorbing aerosols from Nimbus 7/TOMS data. *Journal of Geophysical Research*, 102 (D14), 16 911-16 922, doi:10.1029/96JD03680.
- Hoff, R. J. and S. A. Christopher, 2009: Remote sensing of particulate pollution from space: Have we reached the promised land? *Journal of the Air & Waste Management Association*, 59, 645-675, doi:10.3155/1047-3289.59.6.645.
- Holz, R. E., S. A. Ackerman, F. W. Nagle, R. Frey, S. Dutcher, R. E. Kuehn, M. A. Vaughan, and B. Baum, 2008: Global Moderate Resolution Imaging Spectroradiometer (MODIS) cloud detection and height evaluation using CALIOP. *Journal of Geophysical Research*, 113, D00A19, doi:10.1029/2008JD009837.
- Hutchison, K. D., S. J. Faruqui, and S. Smith, 2008: Improving correlations between MODIS aerosol optical thickness and ground-based PM<sub>2.5</sub> observations through 3D spatial analyses. *Atmospheric Environment*, 42 (3), 530-543, doi:10.1016/j.atmosenv.2007.09.050.
- Hutchison, K. D., S. Smith, and S. J. Faruqui, 2005: Correlating MODIS aerosol optical thickness data with ground-based PM<sub>2.5</sub> observations across Texas for use in a real-time air quality prediction system. *Atmospheric Environment*, 39, 7190-7203, doi:10.1016/j.atmosenv.2005.08.036.
- Justice, C. O., et al., 1998: The Moderate Resolution Imaging Spectroradiometer (MODIS): Land remote sensing for global change research. *IEEE Transactions on Geoscience and Remote Sensing*, 36 (4), 1228-1249.
- Justice, C. O., et al., 2002: The MODIS fire products. *IEEE Transactions on Geoscience and Remote Sensing*, 83, 244-262.
- Justice, C. O., et al., 2013: Land and cryosphere products from Suomi NPP VIIRS: Overview and status. *Journal of Geophysical Research: Atmospheres*, 118, 9753-9765, doi:10.1002/jgrd.50771.
- Kalnay, E., M. Kanamitsu, and W. E. Baker, 1990: Global numerical weather prediction at the National Meteorological Center. *Bulletin of the American Meteorological Society*, 71 (10), 1410-1428, doi:10.1175/1520-0477(1990)071<1410:GNWPAT>2.0.CO;2.
- Kanamitsu, M., 1989: Description of the NMC Global Data Assimilation and Forecasting System. *Weather and Forecasting*, 4 (3), 335-342, doi:10.1175/1520-0434(1989)004<0035:DOTNGD>2.0.CO;2.
- Kanamitsu, M., et al., 1991: Recent changes implemented into the Global Forecast System at NMC. *Weather and Forecasting*, 6 (3), 425-435, doi:10.1175/1520-0434(1991)006<0425:RCIITG>2.0.CO;2.
- Kaufman, Y. J., C. O. Justice, L. P. Flynn, J. D. Kendall, E. M. Prins, L. Giglio, D. E. W. W. P. Menzel, and A. W. Setzer, 1998: Potential global fire monitoring from EOS-MODIS. *Journal of Geophysical Research*, 103 (D24), 32215-32238, doi:10.1029/98JD01644.
- Kaufman, Y. J., D. Tanrè, L. A. Remer, E. F. Vermote, A. Chu, and B. N. Holben, 1997: Operational remote sensing of tropospheric aerosol over land from EOS moderate resolution imaging spectrometer. *Journal of Geophysical Research*, 102 (D14), 17051-17067, doi:10.1029/96JD03988.

- King, M. D., Y. J. Kaufman, D. Tanrè, and T. Nakajima, 1999: Remote sensing of tropospheric aerosols from space: Past, present, and future. *Bulletin of the American Meteorological Society*, 80 (11), 2229-2259, doi:10.1175/1520-0477(1999)080<2229:RSOTAF>2.0.CO;2.
- Lee, K. H., Z. Li, Y. J. Kim, and A. Kokhanovsky, 2009: Atmospheric aerosol monitoring from satellite observations: A history of three decades. *Atmospheric and Biological Environmental Monitoring*, Y. J. Kim, U. Platt, M. B. Gu, and H. Iwahashi, Eds., Springer Netherlands, 13-38, doi:10.1007/978-1-4020-9674-7\_2.
- Li, C., N. C. Hsu, and S.-C. Tsay, 2011: A study on the potential application of satellite data in air quality monitoring and forecasting. *Atmospheric Environment*, 45 (22), 3663-3675, doi:10.1016/j.atmosenv.2011.04.032.
- Martin, R. V., 2008: Satellite remote sensing of surface air quality. *Atmospheric Environment*, 42 (34), 7823-7843, doi:10.1016/j.atmosenv.2008.07.018.
- Masuoka, E., A. Fleig, R. E. Wolfe, and F. Patt, 1998: Key characteristics of MODIS data products. *IEEE Transactions on Geoscience and Remote Sensing*, 36 (4), 1313-1323.
- Pierce, R. B. and T. D. A. Fairlie, 1993: Chaotic advection in the stratosphere: Implications for the dispersal of chemically perturbed air from the polar vortex. *Journal of Geophysical Research*, 98 (D10), 18 589-18 595, doi:10.1029/93JD01619.
- Pierce, R. B., T. D. A. Fairlie, W. L. Grose, R. Swinbank, and A. O'Neill, 1994a: Mixing processes within the polar night jet. *Journal of the Atmospheric Sciences*, 51 (20), 2957-2972, doi:10.1175/1520-0469(1994)051<2957:MPWTPN>2.0.CO;2.
- Pierce, R. B., T. D. A. Fairlie, E. E. Remsber, J. M. R. III, and W. L. Grose, 1997: HALOE observations of the Arctic vortex during the 1997 spring: Horizontal structure in the lower stratosphere. *Geophysical Research Letters*, 24 (22), 2701-2704, doi:10.1029/97GL52833.
- Pierce, R. B., W. L. Grose, J. M. R. III, and A. F. Tuck, 1994b: Evolution of Southern Hemisphere spring air masses observed by HALOE. *Geophysical Research Letters*, 21 (3), 213-216, doi:10.1029/93GL02997.
- Remer, L. A., et al., 2002: Validation of MODIS aerosol retrieval over ocean. *Geophysical Research Letters*, 29 (12), 1618, doi:10.1029/2001GL013204.
- Schaap, M., A. Apituley, R. M. A. Timmermans, R. B. A. Koelmeijer, and G. de Leeuw, 2009: Exploring the relation between aerosol optical depth and PM<sub>2.5</sub> at Cabauw, the Netherlands. *Atmospheric Chemistry and Physics*, 9, 909-925, doi:10.1029/2001GL013204.
- Soja, A. J., T. D. Fairlie, D. J. Westberg, and G. Pouliot, 2012: Biomass burning plume injection height estimates using CALIOP, MODIS and the NASA Langley Trajectory Model, <https://www3.epa.gov/ttnchie1/conference/ei20/session7/asoja.pdf>.
- Stowe, L. L., H. Jacobowitz, G. Ohring, K. R. Knapp, and N. R. Nalli, 2002: The Advanced Very High Resolution Radiometer (AVHRR) Pathfinder Atmosphere (PATMOS) climate dataset: Initial analyses and evaluations. *Journal of Climate*, 15, 1243-1260, doi:10.1175/1520-0442(2002)015<1243:TAVHRR>2.0.CO;2.
- Streets, D. G., et al., 2009: Anthropogenic and natural contributions to regional trends in aerosol optical depth, 1980-2006. *Journal of Geophysical Research*, 114 (D10), D00D18, doi:10.1029/2008JD011624.

- Stein, A.F., Draxler, R.R., Rolph, G.D., Stunder, B.J.B., Cohen, M.D., and Ngan, F., 2015: NOAA's HYSPLIT atmospheric transport and dispersion modeling system, *Bulletin of the American Meteorological Society*, 96, 2059-2077, <http://dx.doi.org/10.1175/BAMS-D-14-00110.1>
- Tanrè, D., Y. J. Kaufman, M. Herman, and S. Mattoo, 1997: Remote sensing of aerosol properties over oceans using the MODIS/EOS spectral radiances. *Journal of Geophysical Research*, 102 (D14), 16 971-16 988, doi:10.1029/96JD03437.
- Torres, O., P. K. Bhartia, J. R. Herman, A. Sinyuk, P. Ginoux, and B. A. Holben, 2002: A long-term record of aerosol optical depth from TOMS observations and comparison to AERONET measurements. *Journal of the Atmospheric Sciences*, 59 (3), 398-413, doi:10.1175/1520-0469(2002)059<0398:ALTROA>2.0.CO;2.
- Wang, J. and S. A. Christopher, 2003: Intercomparison between satellite-derived aerosol optical thickness and PM<sub>2.5</sub> mass: Implications for air quality studies. *Geophysical Research Letters*, 30 (21), 2095, doi:10.1029/2003GL018174.
- Winker, D. M., J. Pelon, and M. P. McCormick, 2003: The CALIPSO mission: Spaceborne lidar for observation of aerosols and clouds, *Proc. SPIE*, 4893, 1-11.
- Winker, D. M., M. A. Vaughan, A. H. Omar, Y. Hu, K. A. Powell, Z. Liu, W. H. Hunt, and S. A. Young, 2009: Overview of the CALIPSO mission and CALIOP data processing algorithms. *Journal of Atmospheric and Oceanic Technology*, 26 (11), 2310-2323, doi:10.1175/2009JTECHA1281.1.
- Zhang, H., R. M. Hoff, and J. A. Engel-Cox, 2009: The relation between Moderate Resolution Imaging Spectroradiometer (MODIS) aerosol optical depth and PM<sub>2.5</sub> over the United States: A geographical comparison by U.S. Environmental Protection Agency regions. *Journal of the Air & Waste Management Association*, 59 (11), 1358-1369, doi:10.3155/1047-3289.59.11.1358.
- Zhao, T. X.-P., I. Laszlo, W. Guo, and A. H. and, 2008: Study of long-term trend in aerosol optical thickness observed from operational AVHRR satellite instrument. *Journal of Geophysical Research*, 113 (D7), D07 201, doi:10.1029/2007JD009061.

| Air Quality Index (AQI) Values        | Levels of Health Concern              | Colors                                 | PM <sub>2.5</sub> values        |
|---------------------------------------|---------------------------------------|--|---------------------------------|
| <i>When the AQI is in this range:</i> | <i>...air quality conditions are:</i> | <i>...as symbolized by this color:</i> | <i>...in µg/m<sup>3</sup> :</i> |
| 0 to 50                               | Good                                  | Green                                  | 0 to 12.0                       |
| 51 to 100                             | Moderate                              | Yellow                                 | 12.1 to 35.4                    |
| 101 to 150                            | Unhealthy for Sensitive Groups        | Orange                                 | 35.5 to 55.4                    |
| 151 to 200                            | Unhealthy                             | Red                                    | 55.5 to 150.4                   |
| 201 to 300                            | Very Unhealthy                        | Purple                                 | 150.5 to 250.4                  |
| 301 to 500                            | Hazardous                             | Maroon                                 | 250.5 to 500                    |

Table 1: AQI, health concern level, color, and corresponding PM<sub>2.5</sub> values. Base table from EPA, amended to include PM<sub>2.5</sub> values that correspond with the AQI range.

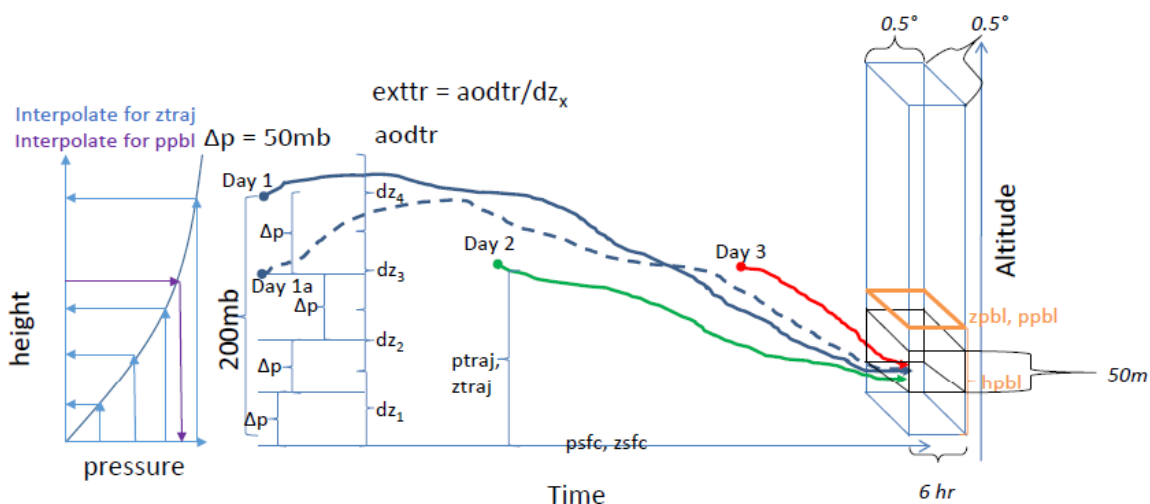


Figure 1: A schematic showing the calculation of the extinction coefficient along a trajectory ( $exttr$ ) and the trajectory aggregation process. Trajectories from three successive days all meet in the same bin. These also lie within the PBL in this schematic. The schematic is not drawn to scale, nor is it the representation of any actual data from this study.

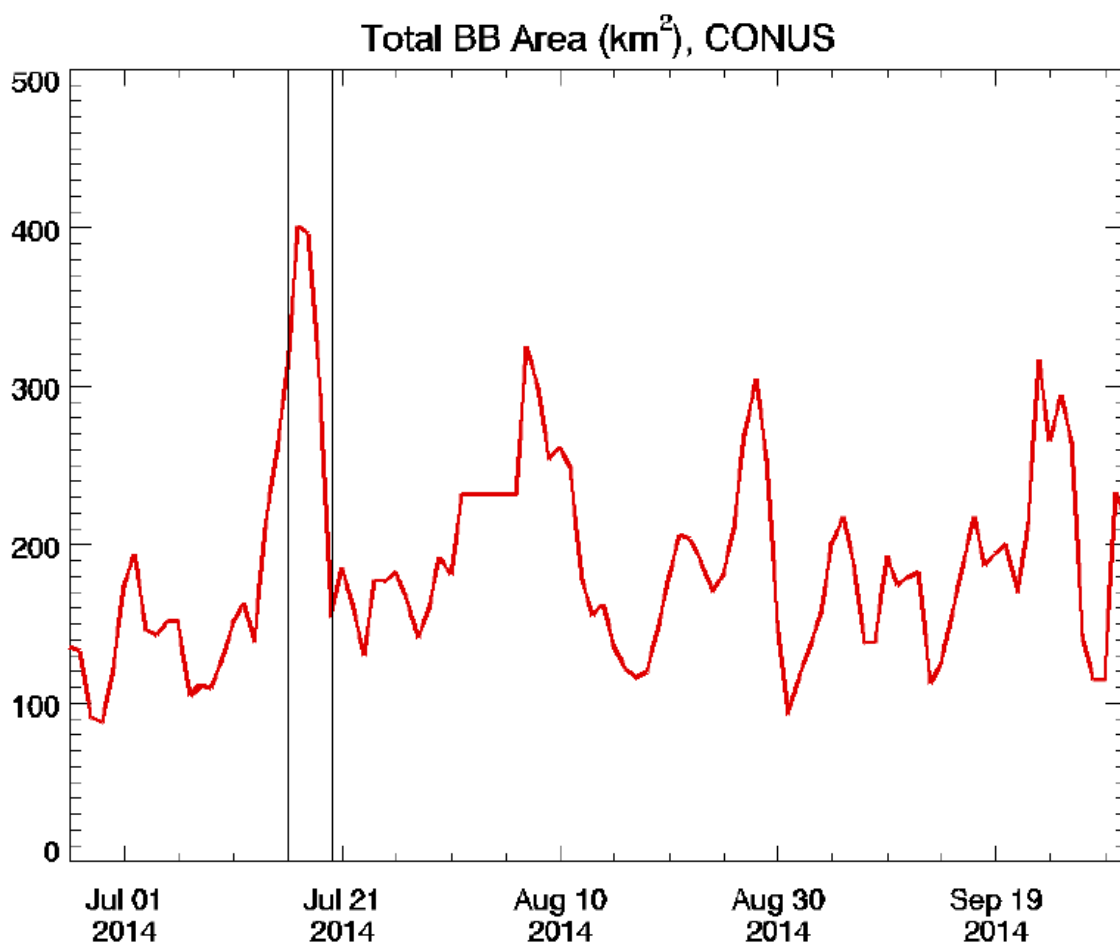


Figure 2: The daily biomass burning area within the CONUS for the summer of 2014. A black box denotes the period July 16 to July 20, containing the two most intense biomass burning days in the CONUS for summer 2014.

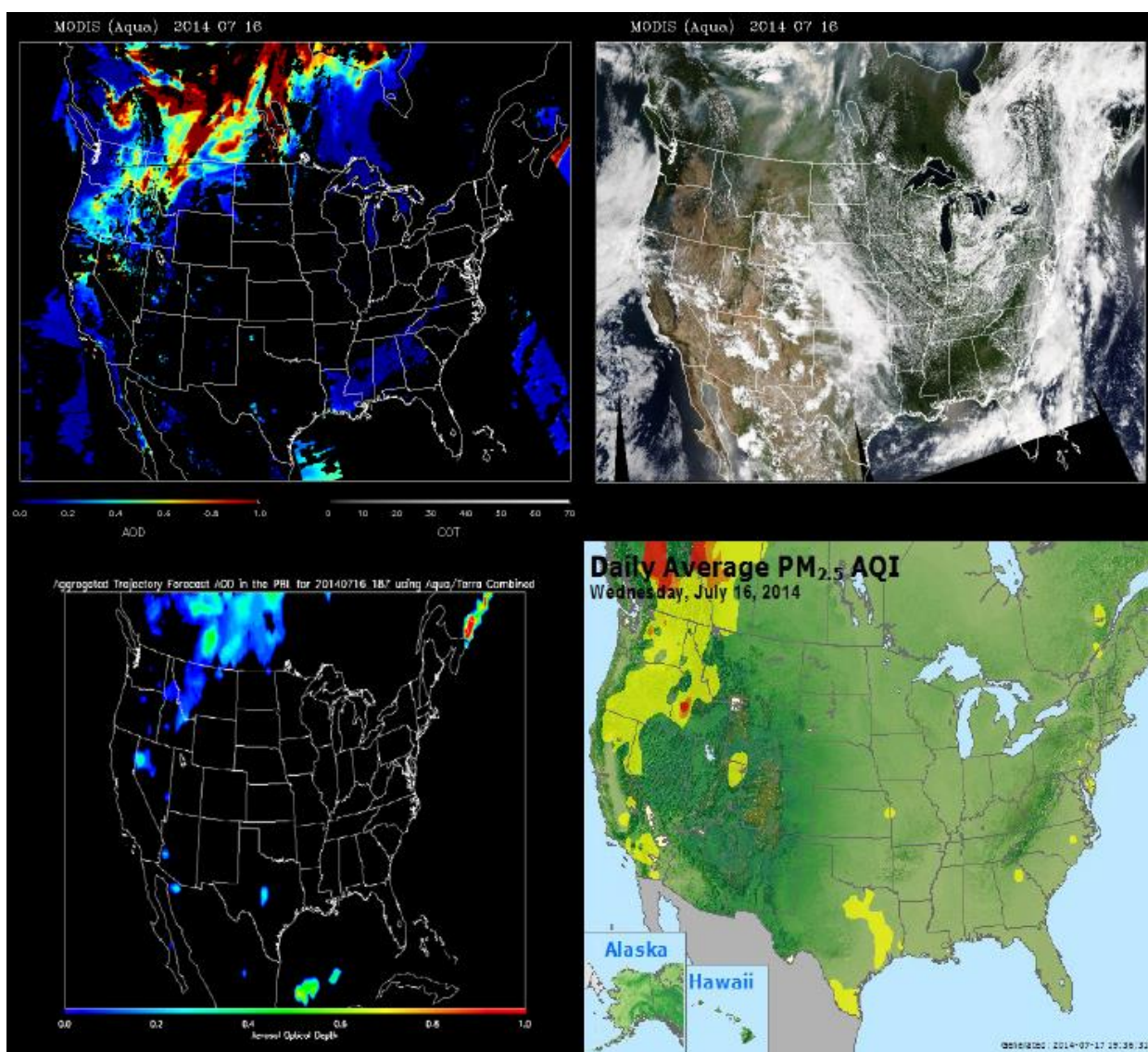


Figure 3: Aqua MODIS 550nm AOD retrieval (top left), Aqua MODIS RGB image (top right), AirNow AQI for PM<sub>2.5</sub> (bottom right), and the 18Z PBL AOD forecast from IDEA-1 (bottom left) for July 16, 2014.

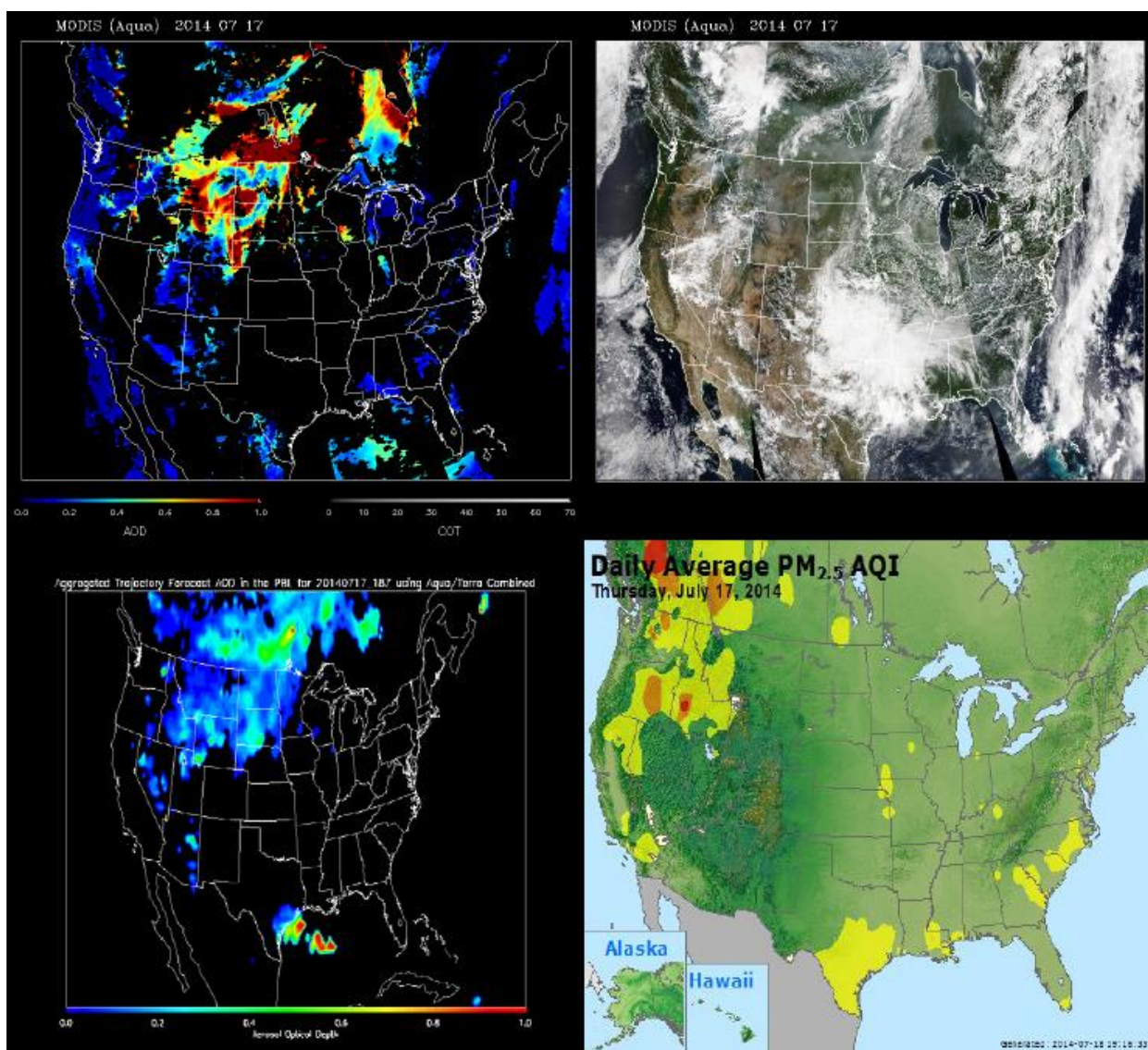


Figure 4: Aqua MODIS 550nm AOD retrieval (top left), Aqua MODIS RGB image (top right), AirNow AQI for PM<sub>2.5</sub> (bottom right), and the 18Z PBL AOD forecast from IDEA-1 (bottom left) for July 17, 2014.

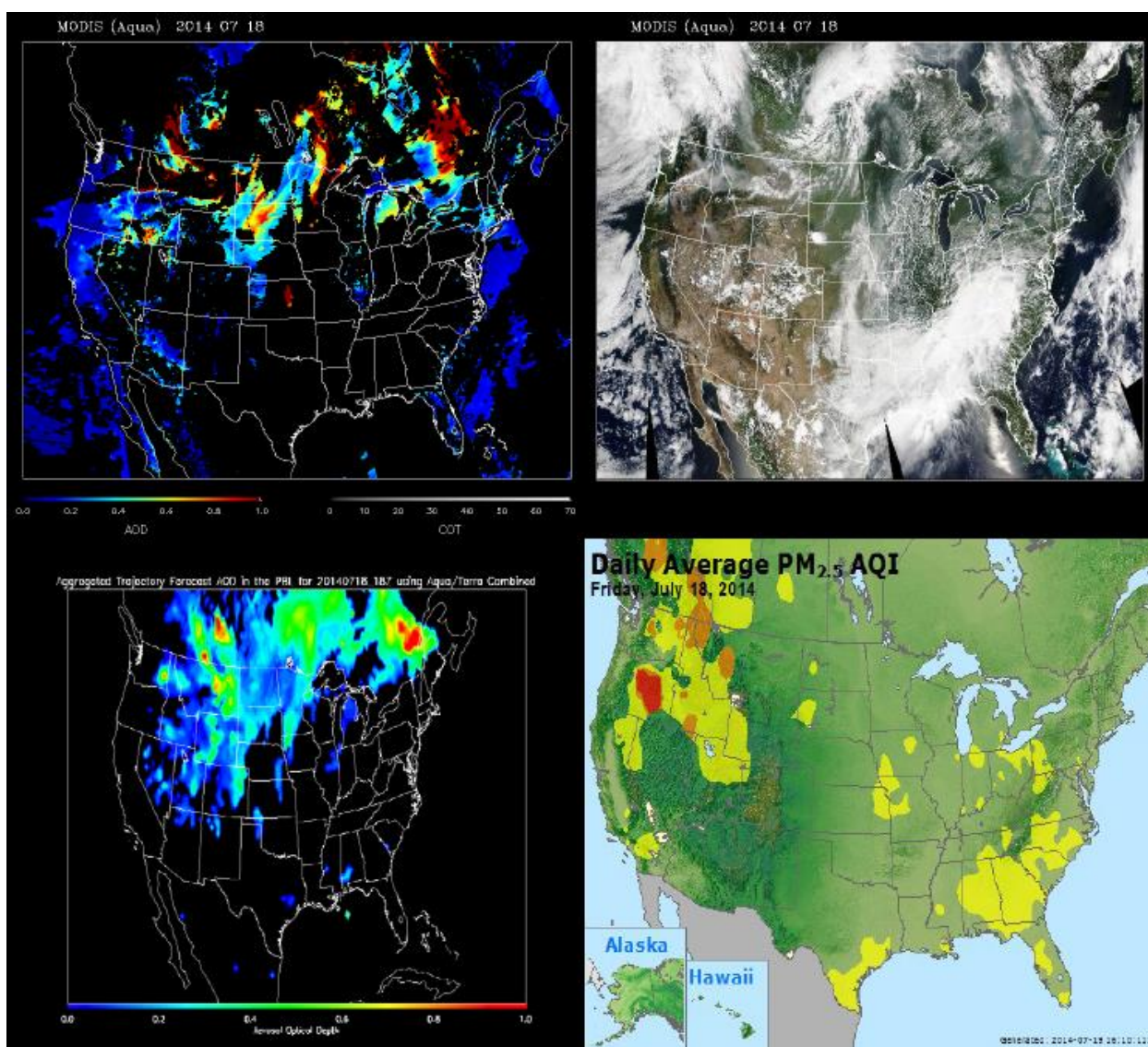


Figure 5: Aqua MODIS 550nm AOD retrieval (top left), Aqua MODIS RGB image (top right), AirNow AQI for PM<sub>2.5</sub> (bottom right), and the 18Z PBL AOD forecast from IDEA-I (bottom left) for July 18, 2014.

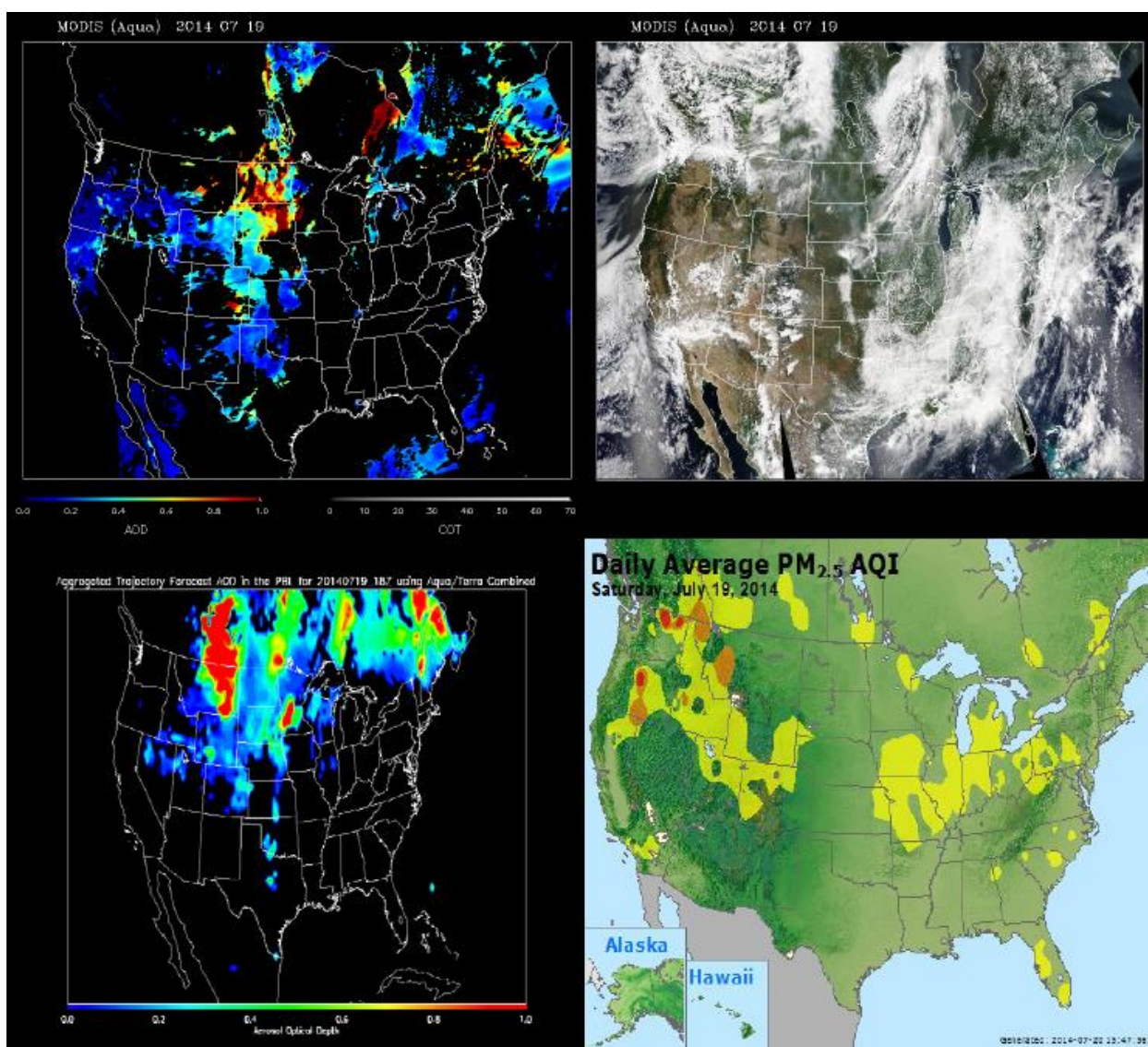


Figure 6: Aqua MODIS 550nm AOD retrieval (top left), Aqua MODIS RGB image (top right), AirNow AQI for PM<sub>2.5</sub> (bottom right), and the 18Z PBL AOD forecast from IDEA-I (bottom left) for July 19, 2014.

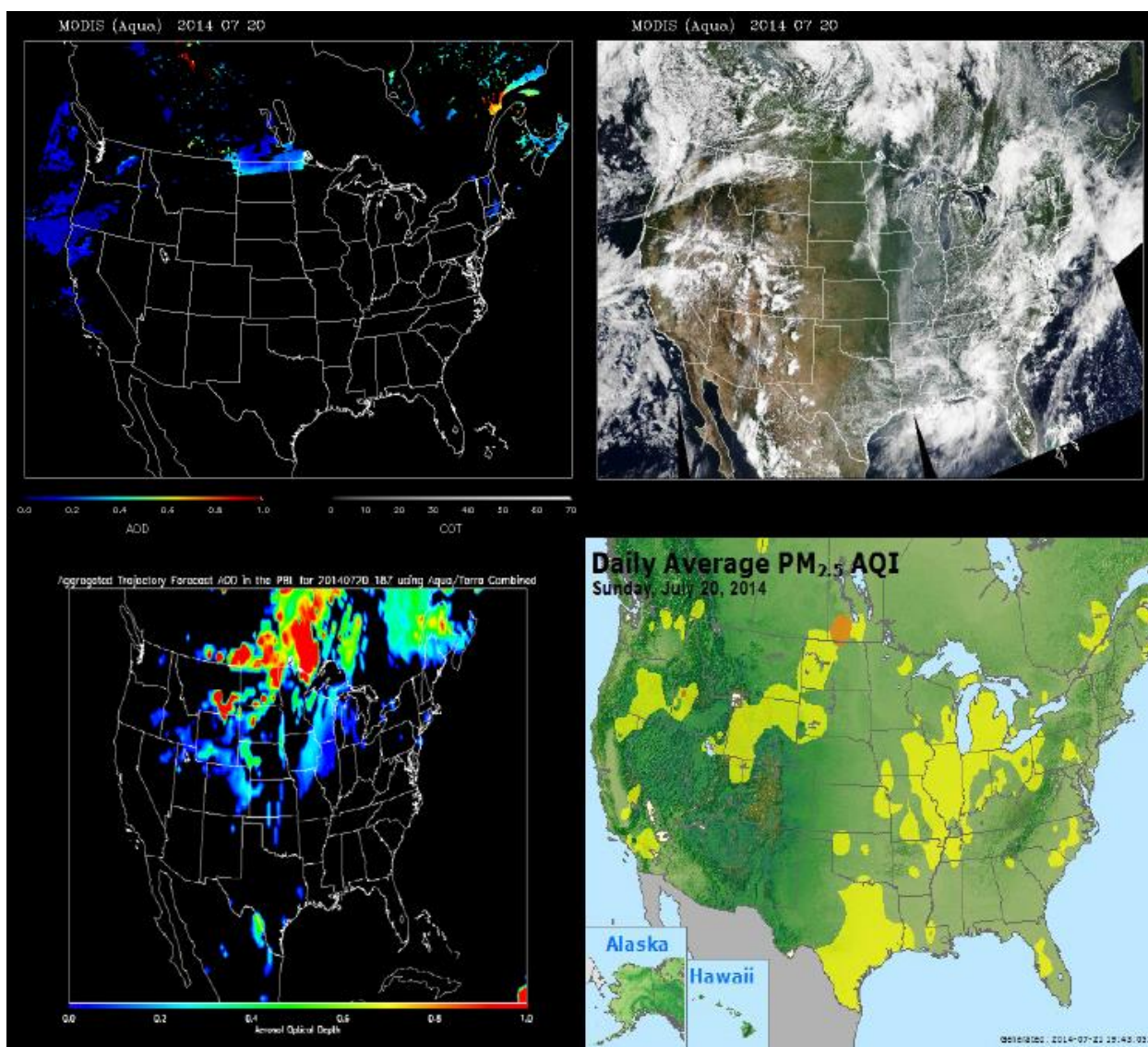


Figure 7: Aqua MODIS 550nm AOD retrieval (top left), Aqua MODIS RGB image (top right), AirNow AQI for  $PM_{2.5}$  (bottom right), and the 18Z PBL AOD forecast from IDEA-1 (bottom left) for July 20, 2014. Note a lack of Aqua MODIS AOD retrievals over the United States for this day.

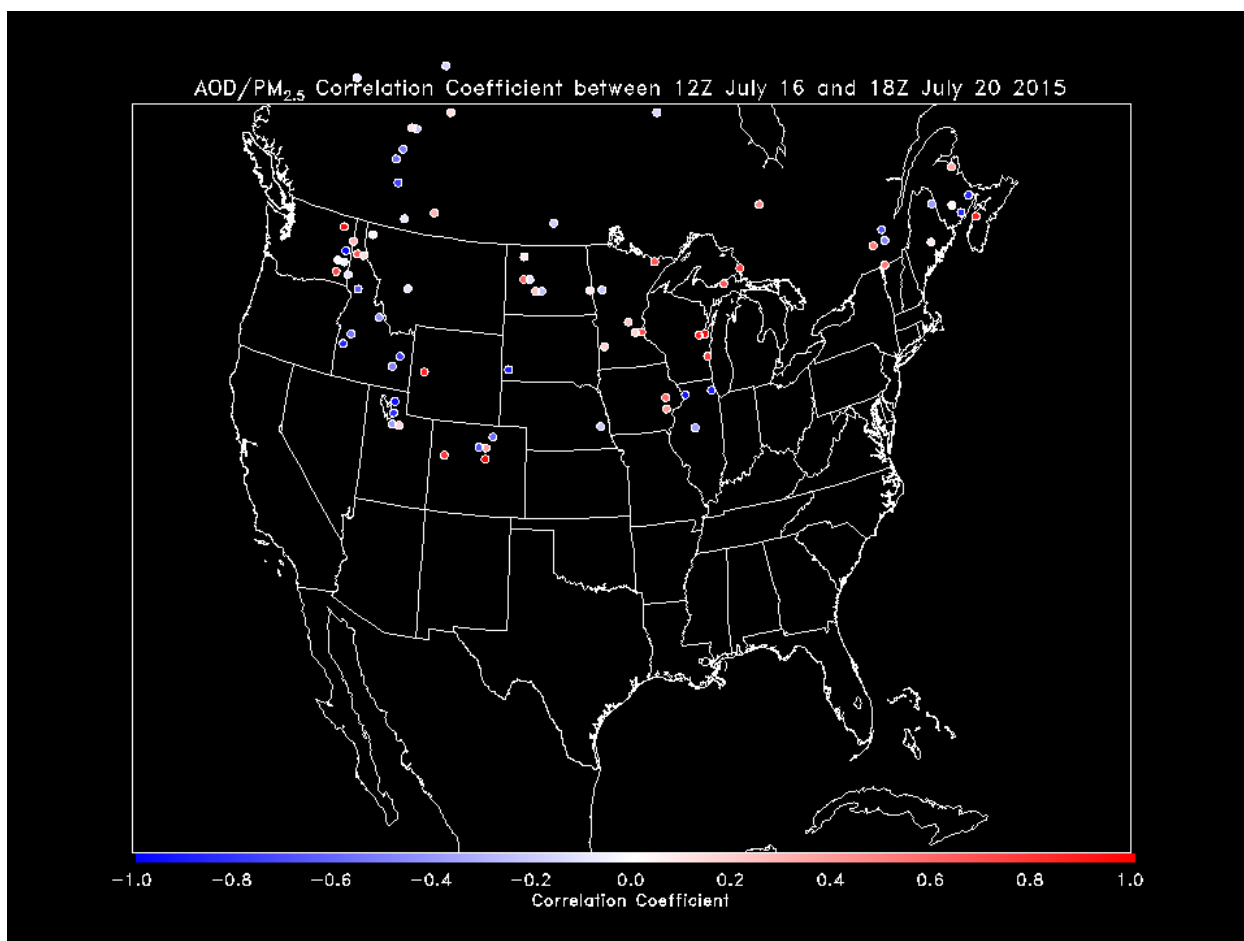


Figure 8: Correlation coefficient between  $PM_{2.5}$  and AOD for all AirNow  $PM_{2.5}$  sites with at least three coincident valid AOD forecasts.

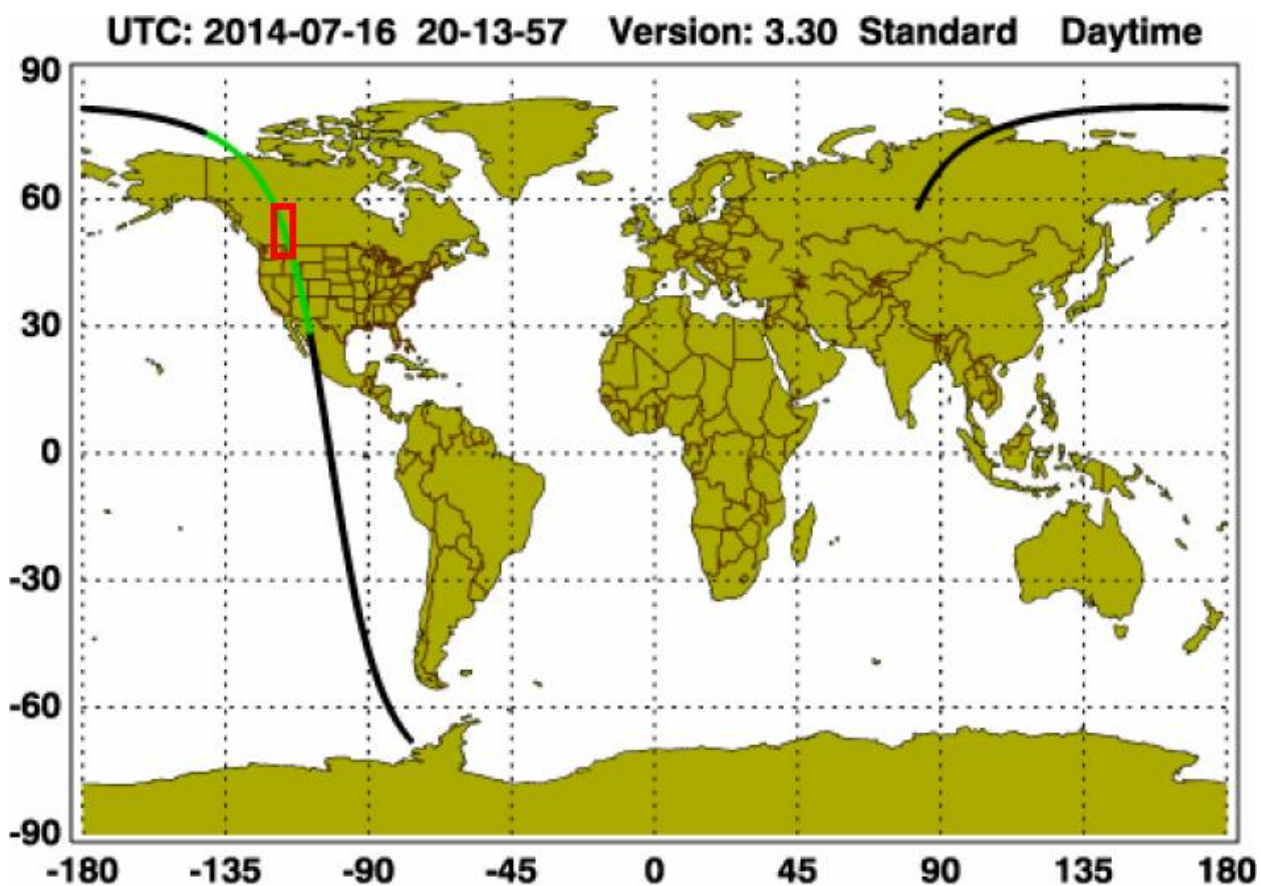


Figure 9: CALIPSO track map for the western North American daytime overpass on July 16, 2014. The green shaded path denotes the portion of the track shown in Figure 10. The red box outlines the domain of the IDEA-I cross-section in Figure 11.

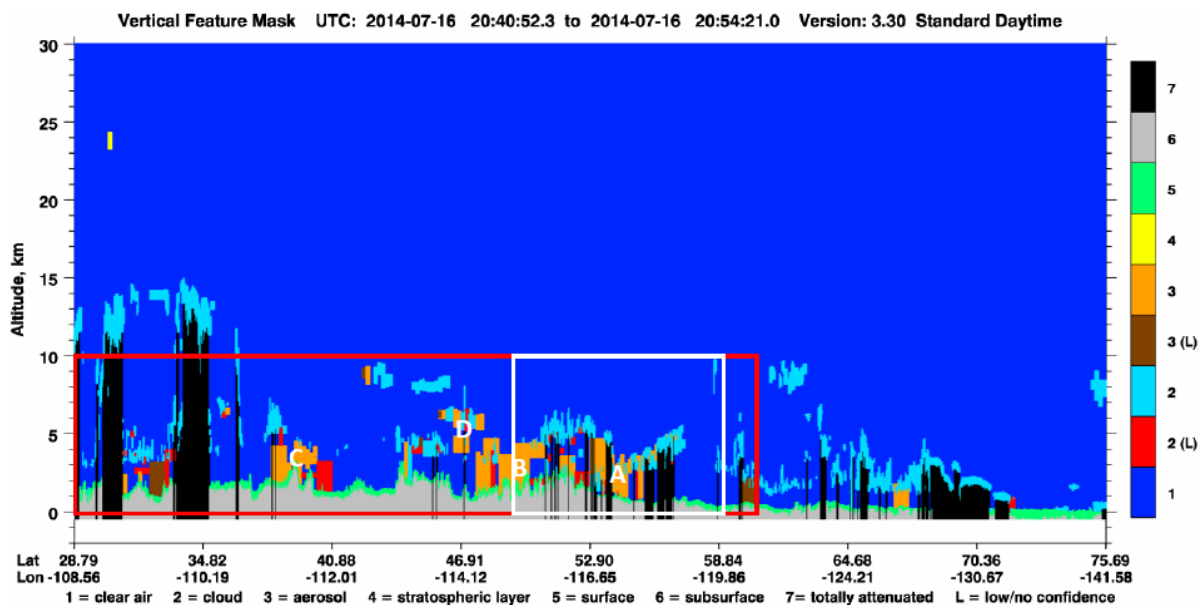


Figure 10: CALIOP vertical feature mask image taken along the green shaded path in Figure 9. South and east are left. Letters denote features of interest. The red box delineates the latitude and height extent of the IDEEA-I forecast cross-sections. The white box denotes the latitude and longitude range corresponding to the forecast cross-section in Figure 11.

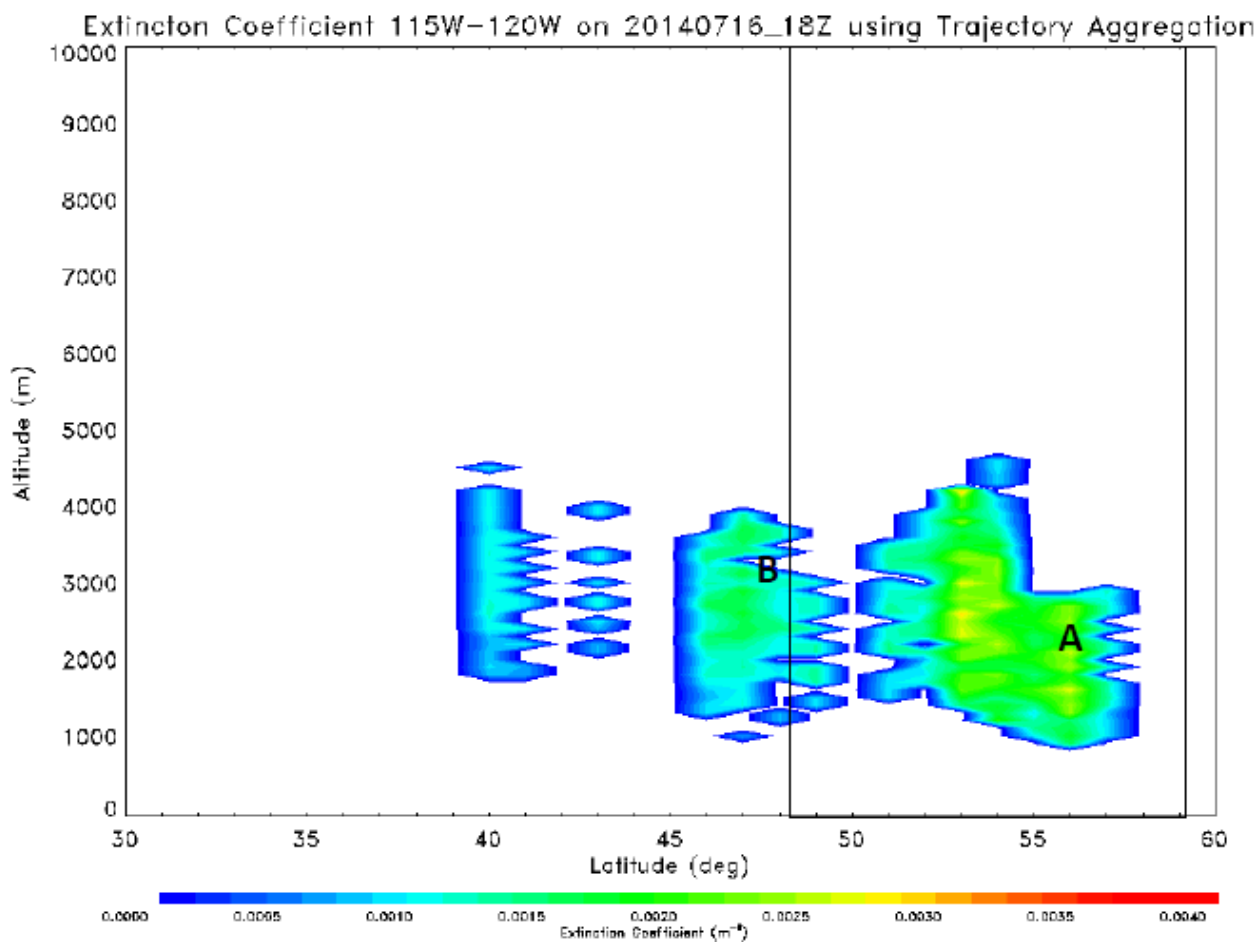


Figure 11: IDEA-I extinction coefficient cross-section for the latitude range 115W to 120W at 18Z on July 16, 2014. The black box denotes the latitude range 115W to 120W spans in Figure 10. Letters denote features which correspond to the same letters in Figure 10.

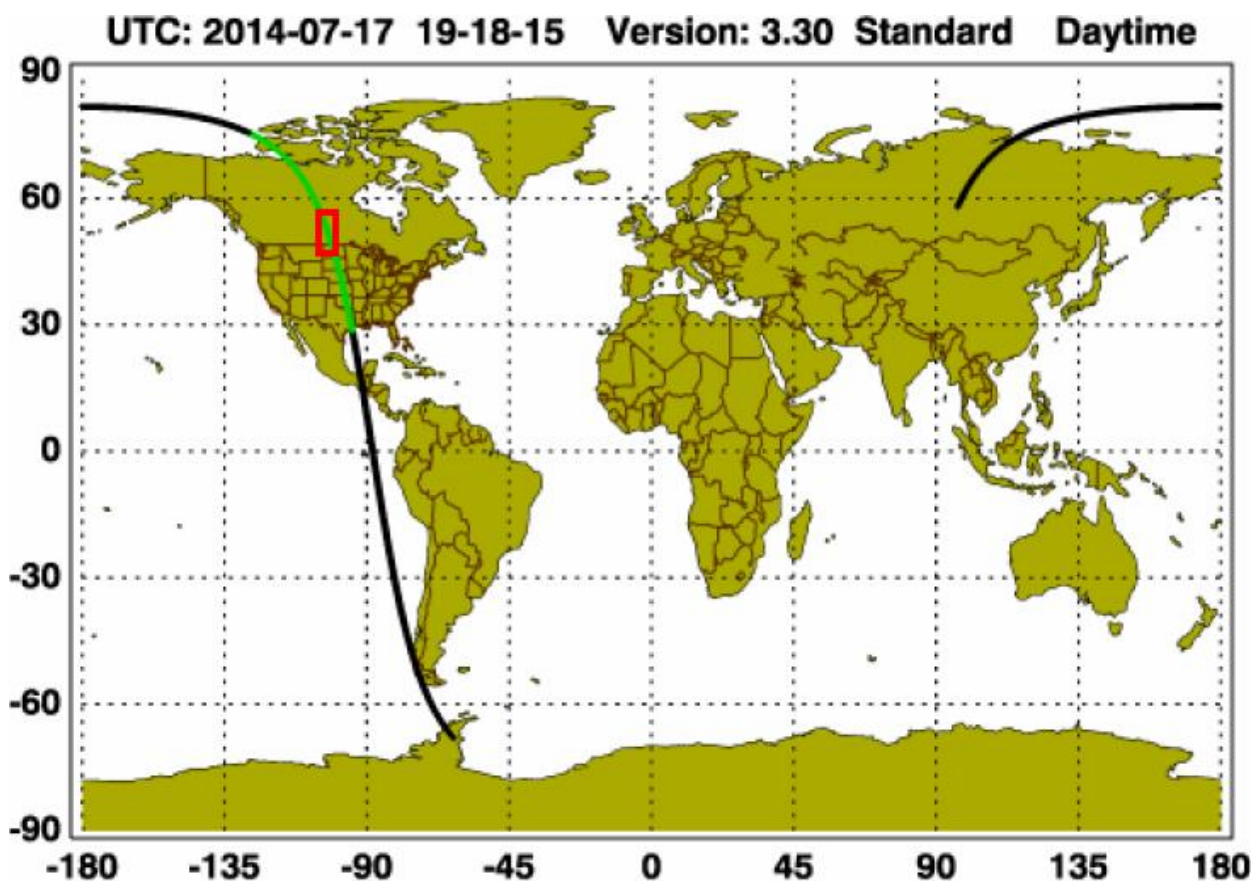


Figure 12: CALIPSO track map for the central North American daytime overpass on July 17, 2014. The green shaded path denotes the portion of the track shown in Figure 13. The red box outlines the domain of the IDEA-I cross-section in Figure 14.

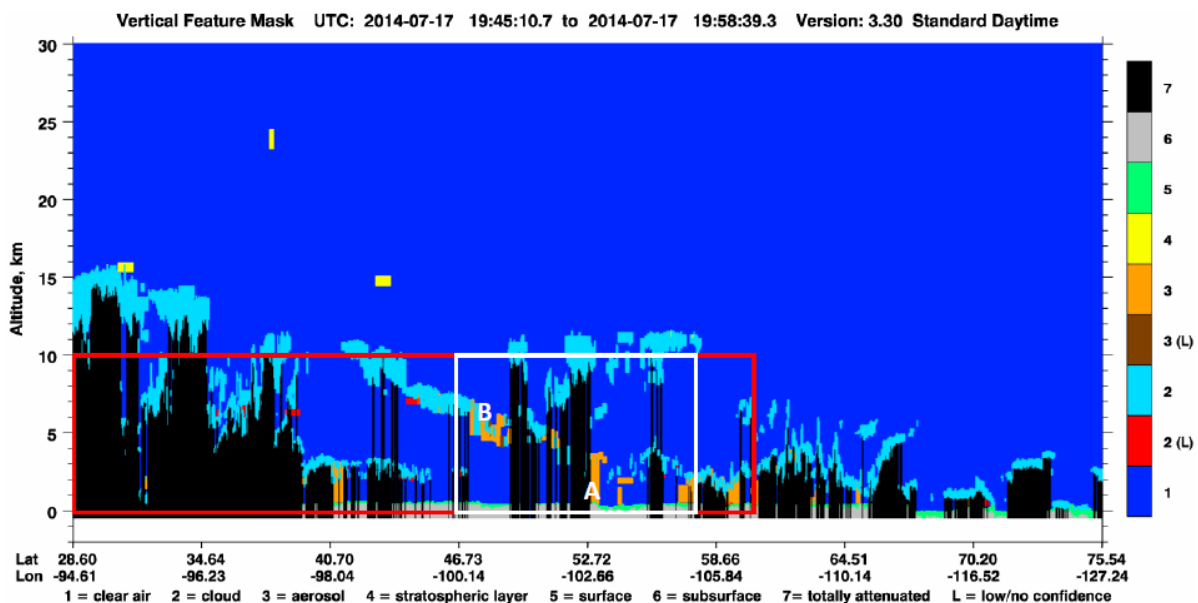


Figure 13: CALIOP vertical feature mask image taken along the green shaded path in Figure 12. South and east are left. Letters denote features of interest. The red box delineates the latitude and height extent of the IDEA-I forecast cross-sections. The white box denotes the latitude and longitude range corresponding to the forecast cross-section in Figure 14.

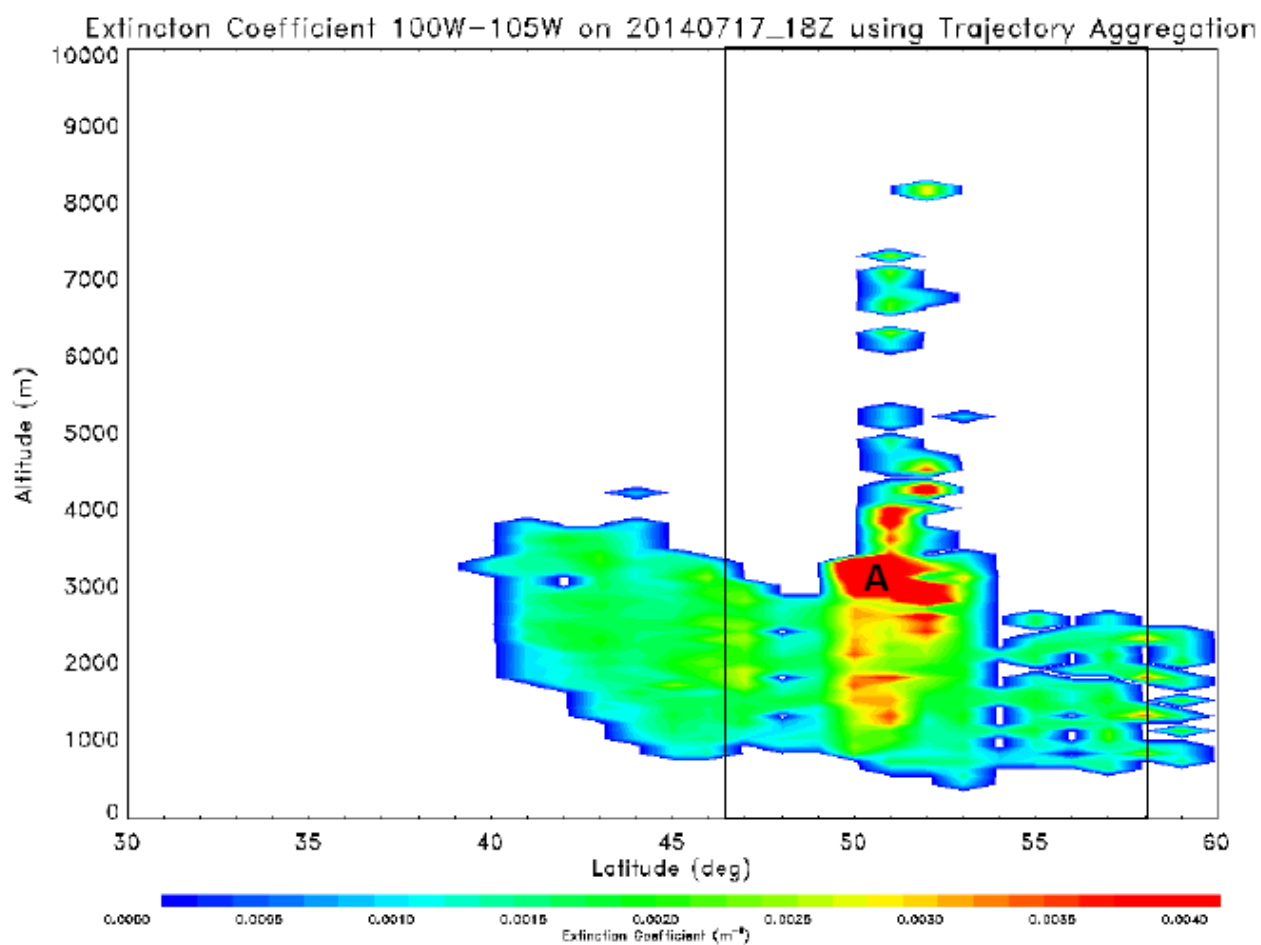


Figure 14: IDEA-I extinction coefficient cross-section for the latitude range 100W to 105W at 18Z on July 17, 2014. The black box denotes the latitude range 100W to 105W spans in Figure 13. Letters denote features which correspond to the same letters in Figure 13.

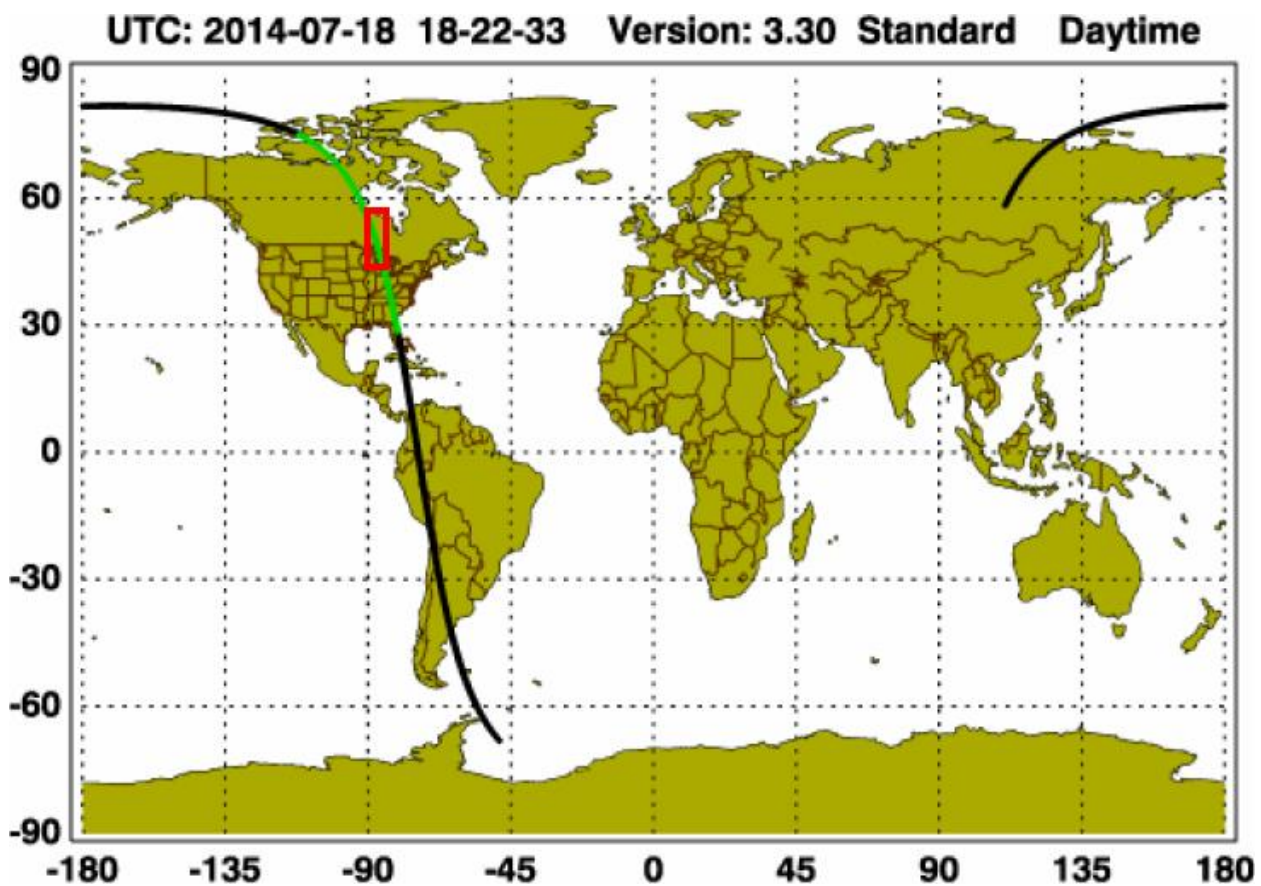


Figure 15: CALIPSO track map for the eastern North American daytime overpass on July 18, 2014. The green shaded path denotes the portion of the track shown in Figure 16. The red box outlines the domain of the IDEA-I cross-section in Figure 17.

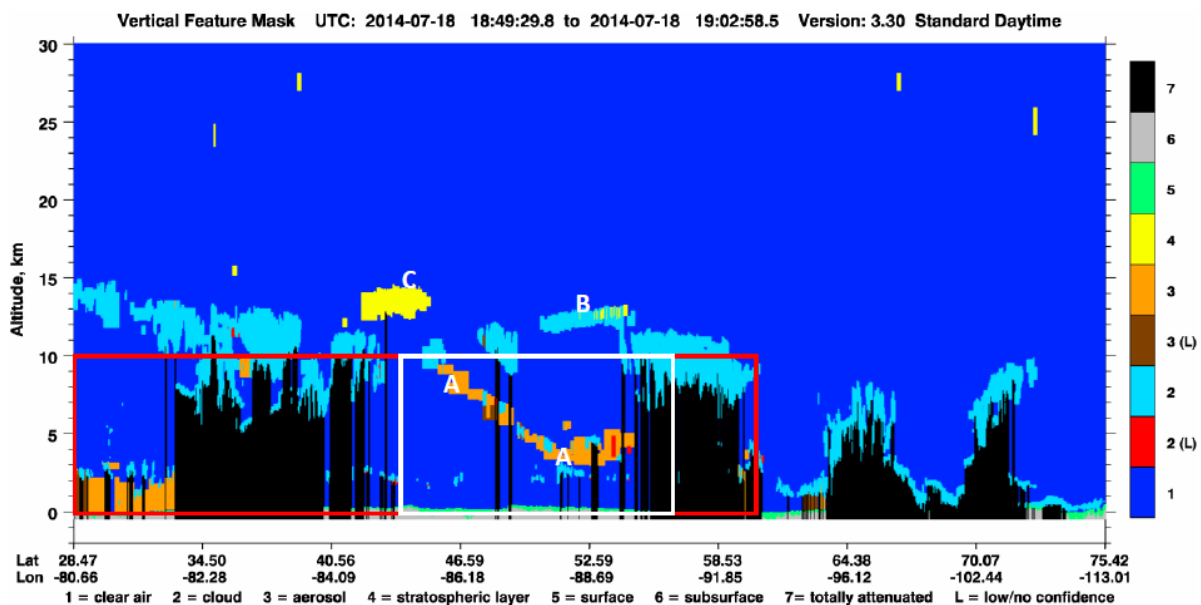


Figure 16: CALIOP vertical feature mask image taken along the green shaded path in Figure 15. South and east are left. Letters denote features of interest. The red box delineates the latitude and height extent of the IDEA-I forecast cross-sections. The white box denotes the latitude and longitude range for the forecast cross-section in Figure 17.

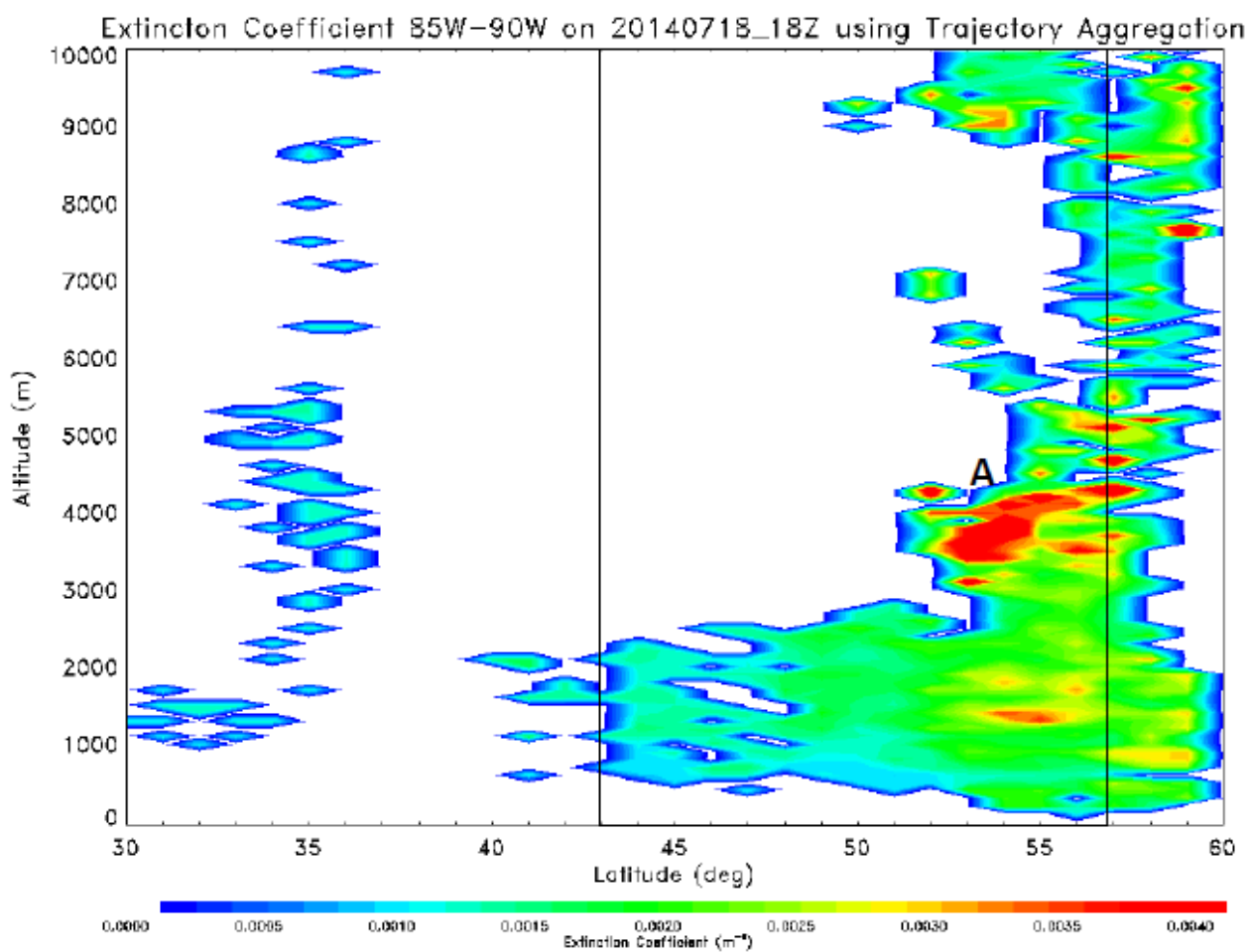


Figure 17: IDEA-I extinction coefficient cross-section for the latitude range 85W to 90W at 18Z on July 18, 2014. The black box denotes the latitude range 85W to 90W spans in Figure 16. Letters denote features which correspond to the same letters in Figure 16.

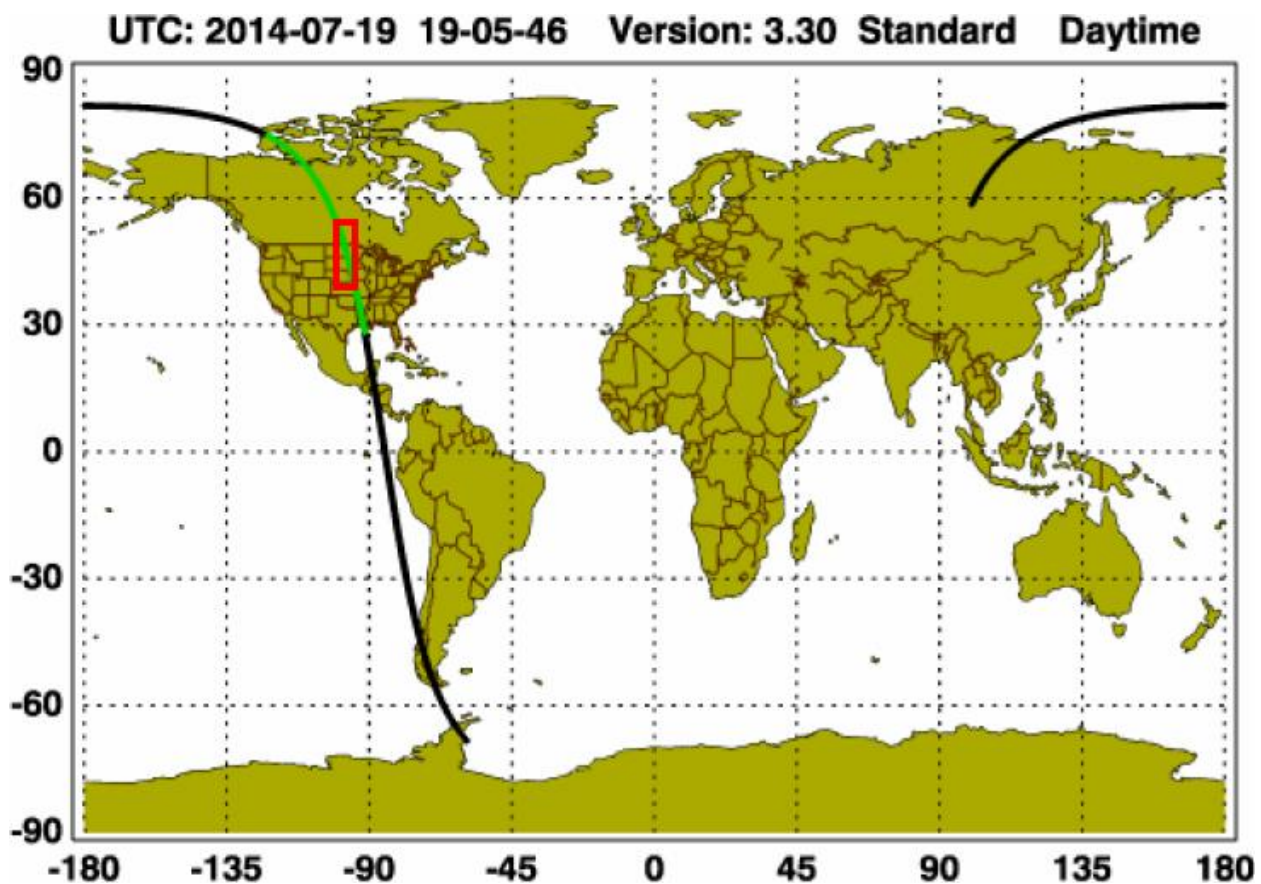


Figure 18: CALIPSO track map for the central North American daytime overpass on July 19, 2014. The green shaded path denotes the portion of the track shown in Figure 19. The red box outlines the domain of the IDEA-I cross-section in Figure 20.

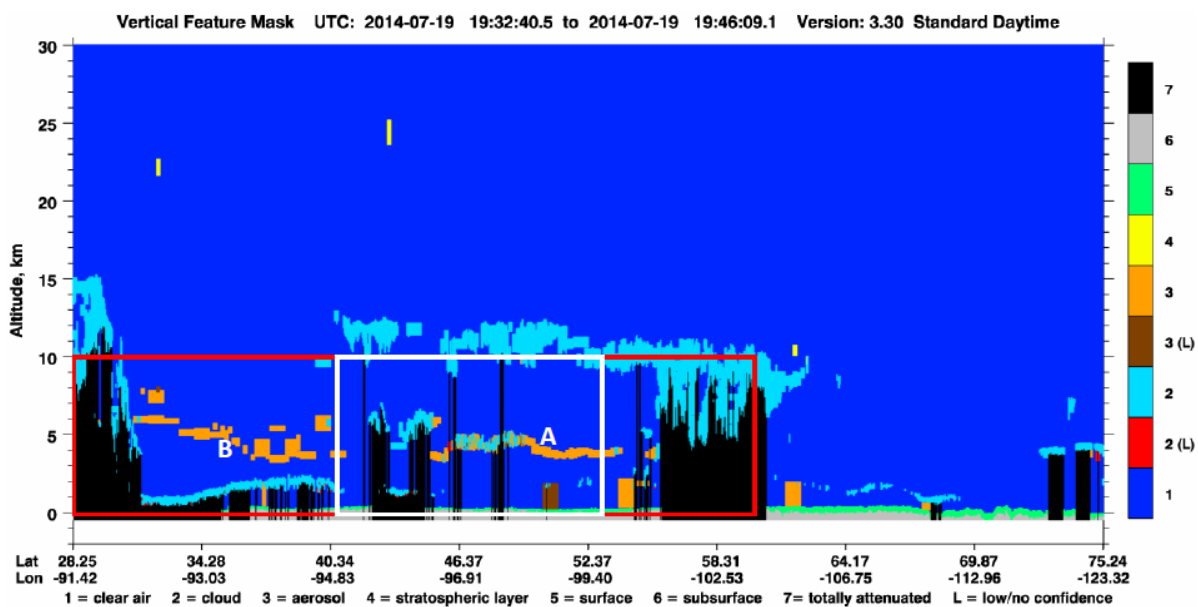


Figure 19: CALIOP vertical feature mask image taken along the green shaded path in Figure 18. South and east are left. Letters denote features of interest. The red box delineates the latitude and height extent of the IDEA-I forecast cross-sections. The white box denotes the latitude and longitude range for the forecast cross-section in Figure 20.

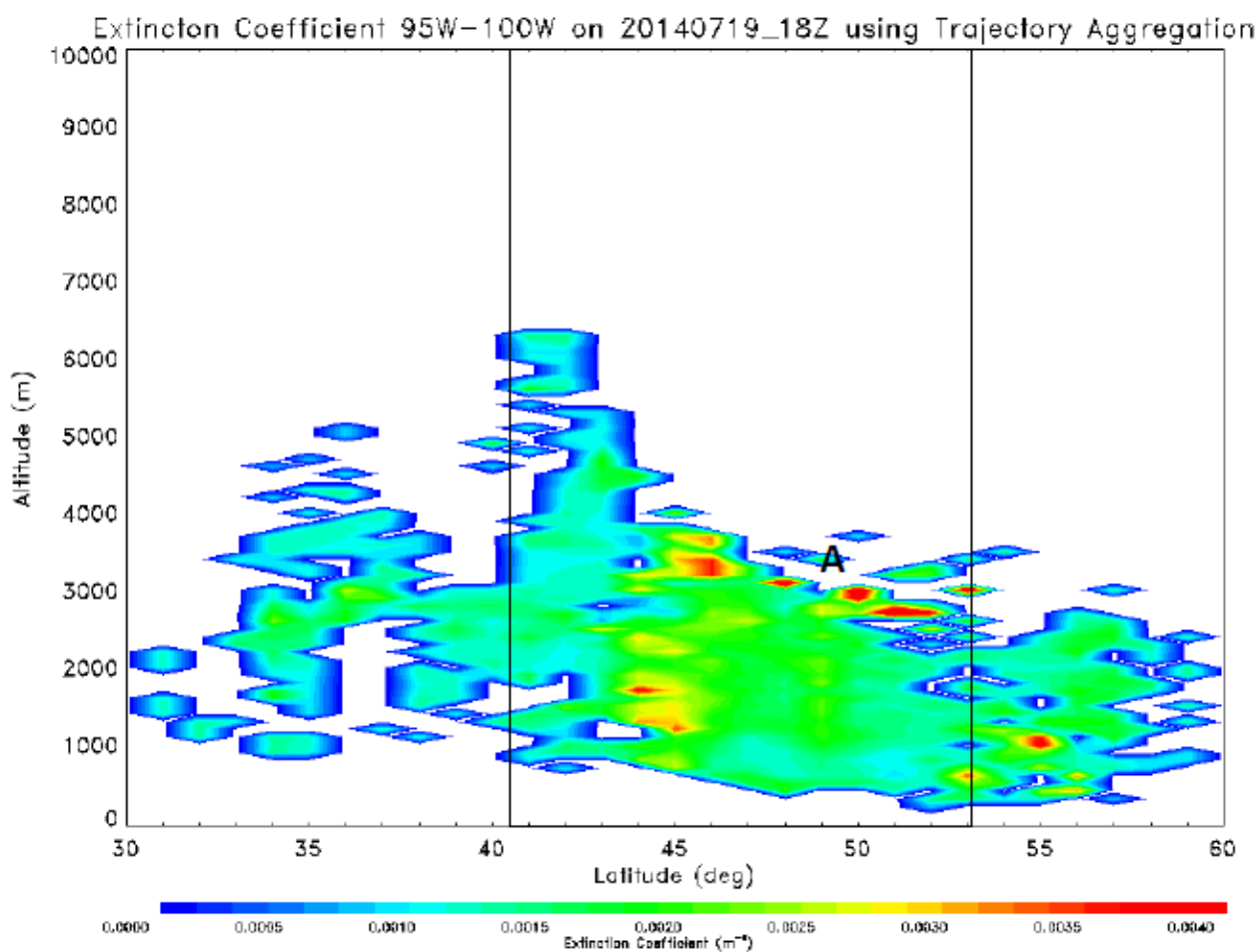


Figure 20: IDEA-I extinction coefficient cross-section for the latitude range 95W to 100W at 18Z on July 19, 2014. The black box denotes the latitude range 95W to 100W spans in Figure 19. Letters denote features which correspond to the same letters in Figure 19.

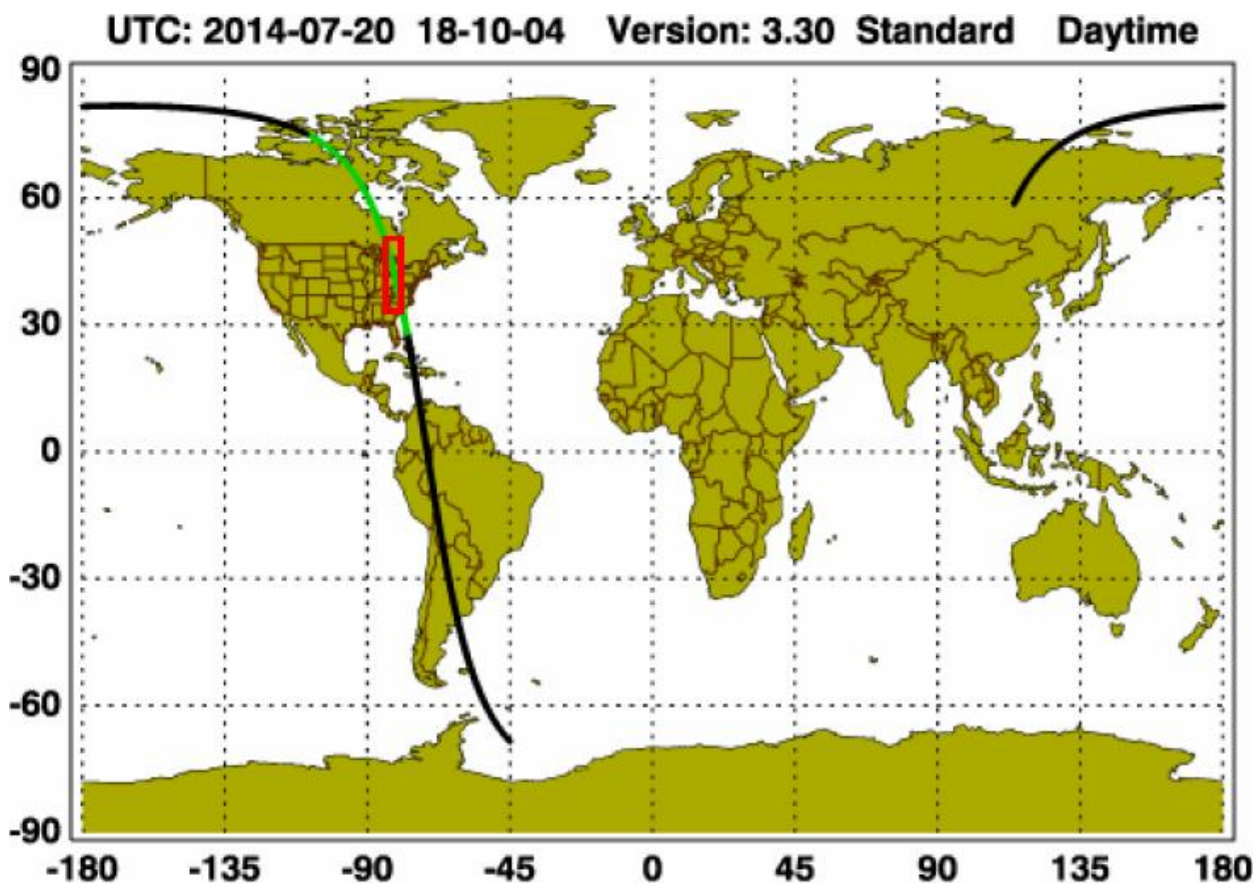


Figure 21: CALIPSO track map for the eastern North American daytime overpass on July 20, 2014. The green shaded path denotes the portion of the track shown in Figure 22. The red box outlines the domain of the IDEA-I cross-section in Figure 23.

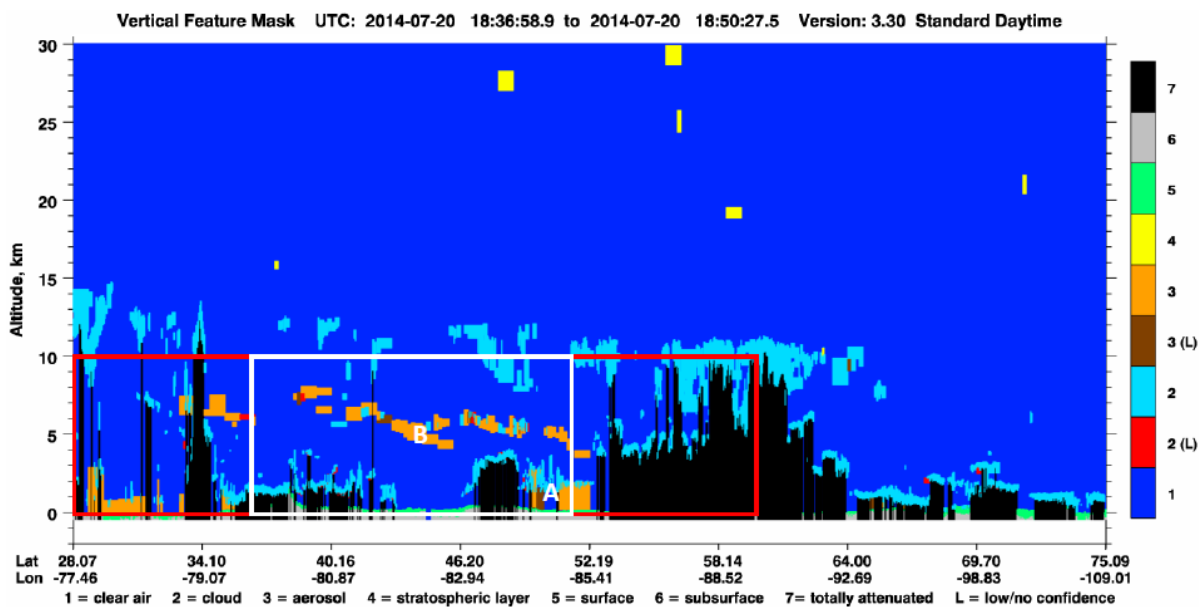


Figure 22: CALIOP vertical feature mask image taken along the green shaded path in Figure 21. South and east are left. Letters denote features of interest. The red box delineates the latitude and height extent of the IDEA-I forecast cross-sections. The white box denotes the latitude and longitude range for the forecast cross-section in Figure 23.

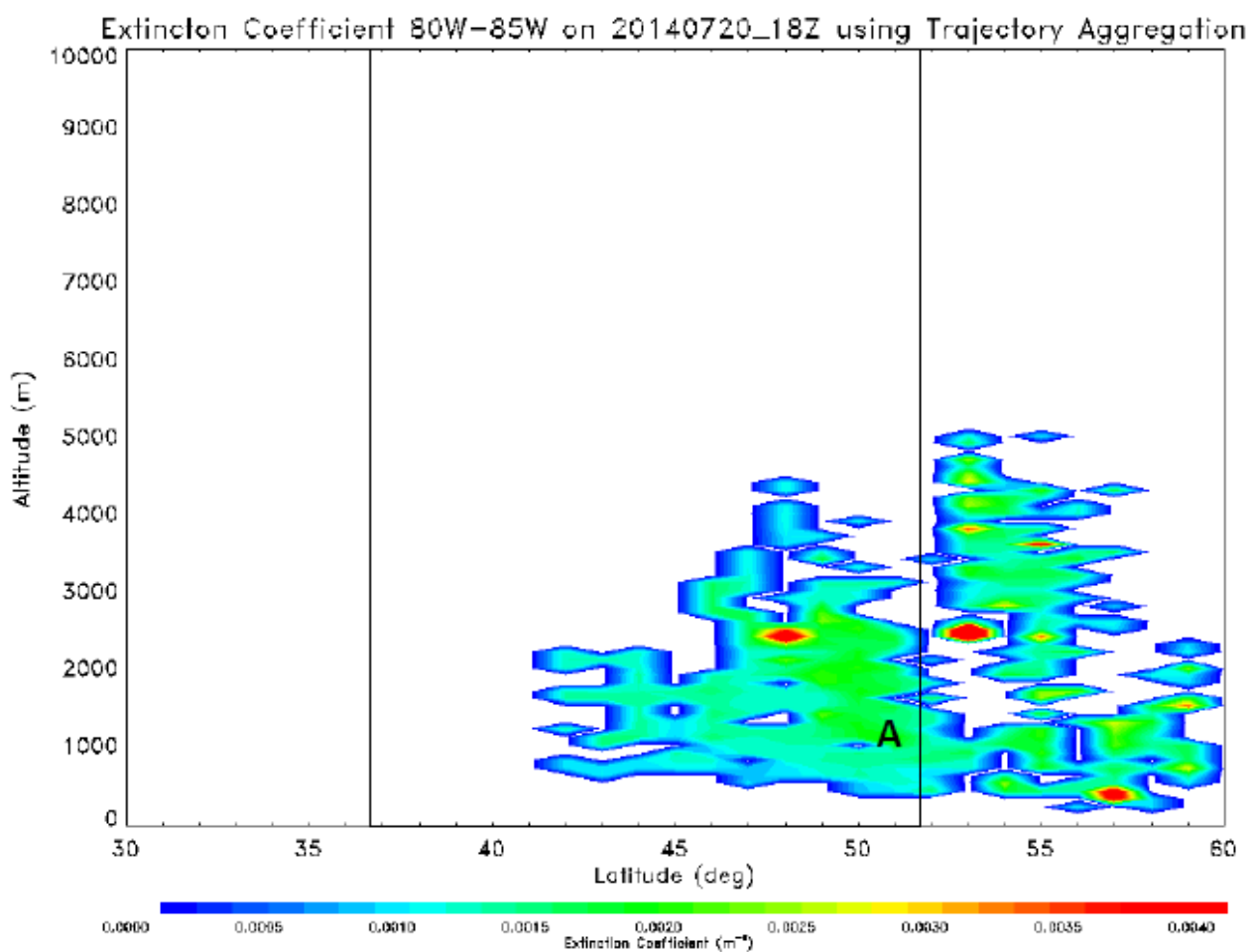


Figure 23: IDEA-I extinction coefficient cross-section for the latitude range 80W to 85W at 18Z on July 20, 2014. The black box denotes the latitude range 80W to 85W spans in Figure 22. Letters denote features which correspond to the same letters in Figure 22.

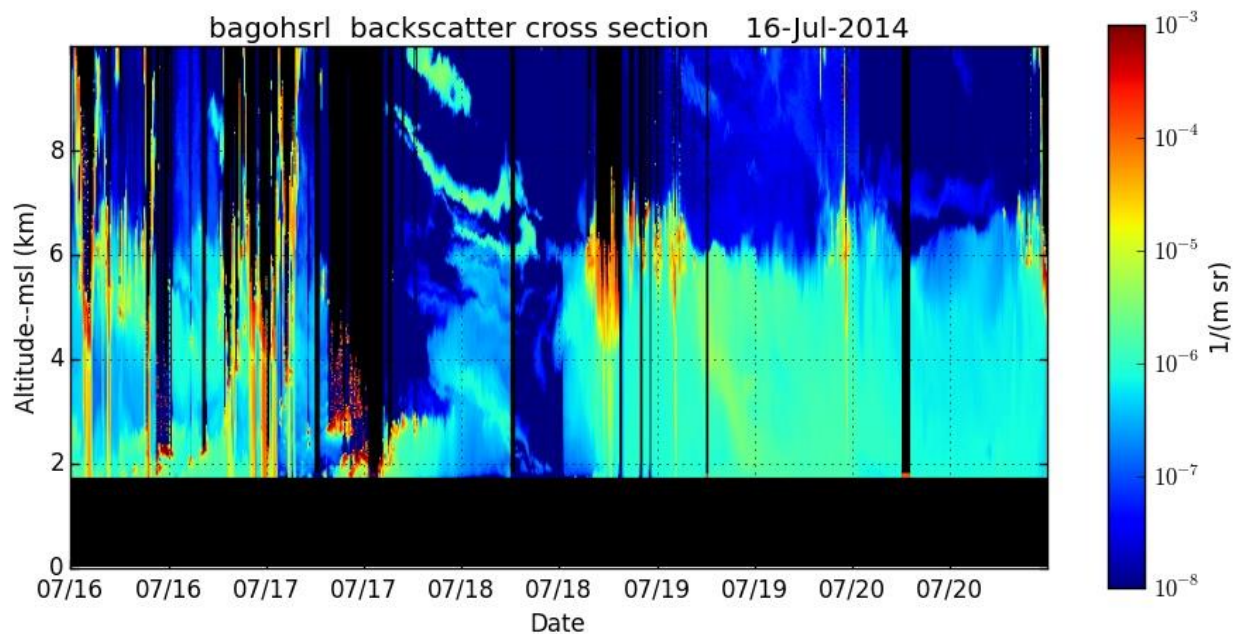


Figure 24: UW-HSRL backscatter image from between 00Z July 16, 2014 to 00Z July 21, 2014. Image obtained from the University of Wisconsin Lidar Group's HSRL data web page for FRAPPE: BAO tower – Erie, CO. [[http://hsrl.ssec.wisc.edu/by\\_site/23/bscat/2014/07/](http://hsrl.ssec.wisc.edu/by_site/23/bscat/2014/07/)]

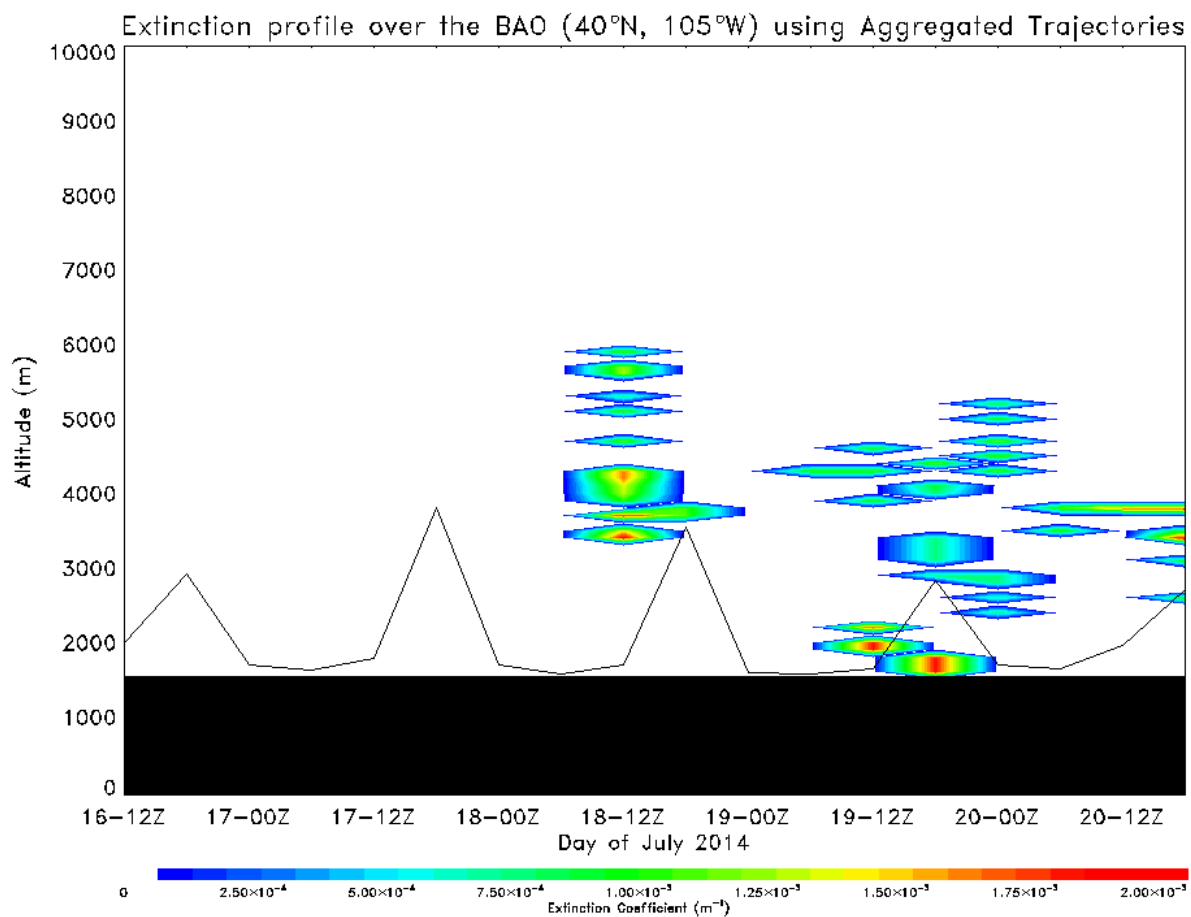


Figure 25: IDEA-I forecast extinction coefficient profile for the time period starting 12Z July 16, 2014 and ending 00Z July 21, 2014.